

Impaired immune signaling and changes in the lung microbiome precede secondary bacterial pneumonia in COVID-19

Alexandra Tsitsiklis

University of California, San Francisco <https://orcid.org/0000-0003-3467-1171>

Beth Zha

University of California, San Francisco

Ashley Byrne

Chan Zuckerberg Biohub <https://orcid.org/0000-0002-2177-924X>

Catherine DeVoe

University of California, San Francisco

Sophia Levan

University of California, San Francisco

Elze Rackaityte

University of California, San Francisco

Sara Sunshine

University of California, San Francisco

Eran Mick

University of California, San Francisco <https://orcid.org/0000-0002-7299-808X>

Rajani Ghale

University of California, San Francisco

Alejandra Jauregui

University of California, San Francisco

Norma Neff

Chan Zuckerberg Biohub <https://orcid.org/0000-0001-7141-5420>

Aartik Sarma

University of California, San Francisco <https://orcid.org/0000-0002-7508-7345>

Paula Serpa

University of California, San Francisco

Thomas Deiss

University of California, San Francisco

Amy Kistler

Chan Zuckerberg Biohub

Sidney Carrillo

University of California, San Francisco

K. Mark Ansel

University of California, San Francisco <https://orcid.org/0000-0003-4840-9879>

Aleksandra Leligdowicz

University of California, San Francisco

Stephanie Christenson

University of California, San Francisco

Norman Jones

University of California, San Francisco

Bing Wu

Genentech, Inc

Spyros Darmanis

Genentech, Inc

Michael Matthay

University of California, San Francisco <https://orcid.org/0000-0003-3039-8155>

Susan Lynch

University of California, San Francisco <https://orcid.org/0000-0001-5695-7336>

Joseph DeRisi

University of California, San Francisco

COMET Consortium

University of California, San Francisco

Carolyn Hendrickson

University of California, San Francisco

Kirsten Kangelaris

University of California, San Francisco

Matthew Krummel

University of California, San Francisco <https://orcid.org/0000-0001-7915-3533>

Prescott Woodruff

University of California, San Francisco

David Erle

University of California, San Francisco <https://orcid.org/0000-0002-2171-0648>

Oren Rosenberg

University of California, San Francisco <https://orcid.org/0000-0002-5736-4388>

Carolyn Calfee

University of California, San Francisco

Charles Langelier (✉ Chaz.Langelier@ucsf.edu)

University of California, San Francisco <https://orcid.org/0000-0002-6708-4646>

Article

Keywords: COVID-19, SARS-CoV-2, secondary bacterial pneumonia, VAP, metagenomics, 41 scRNA-seq

Posted Date: April 23rd, 2021

DOI: <https://doi.org/10.21203/rs.3.rs-380803/v1>

License:  This work is licensed under a Creative Commons Attribution 4.0 International License.

[Read Full License](#)

1 **Title: Impaired immune signaling and changes in the lung microbiome precede secondary**
2 **bacterial pneumonia in COVID-19**

3

4 **Authors:**

5 [†]Alexandra Tsitsiklis¹, [†]Beth Shoshana Zha², [†]Ashley Byrne³, [†]Catherine Devoe¹, [#]Sophia Levan⁴,
6 [#]Elze Rackaityte⁵, Sara Sunshine⁵, Eran Mick^{1,2,3}, Rajani Ghale^{1,2}, Alejandra Jauregui², Aartik
7 Sarma², Norma Neff³, Paula Hayakawa Serpa¹, Thomas J. Deiss², Amy Kistler³, Sidney Carrillo²,
8 K. Mark Ansel^{6,7}, Aleksandra Leligdowicz², Stephanie Christenson², Norman Jones⁸, Bing Wu⁹,
9 Spyros Darmanis⁹, Michael A. Matthay², Susan V. Lynch^{10,11}, Joseph L. DeRisi^{3,5}, COMET
10 Consortium+, Carolyn M. Hendrickson², Kirsten N. Kangelaris⁴, Matthew F. Krummel¹², Prescott
11 G. Woodruff^{2,7}, David J. Erle^{4,13,14}, Oren Rosenberg¹, Carolyn S. Calfee², *Charles R. Langlier^{1,3}

12

13 ^{†#}equal contributions

14

15 **Affiliations:**

16 ¹Department of Medicine, Division of Infectious Diseases, University of California San Francisco,
17 San Francisco, CA, USA

18 ²Department of Medicine, Division of Pulmonary, Critical Care, Allergy and Sleep Medicine,
19 University of California San Francisco, San Francisco, CA, USA

20 ³Chan Zuckerberg Biohub, San Francisco, CA, USA

21 ⁴Department of Medicine, University of California San Francisco, San Francisco, CA, USA

22 ⁵Department of Biochemistry and Biophysics, University of California San Francisco, San
23 Francisco, CA, USA

24 ⁶Department of Microbiology and Immunology, University of California, San Francisco, CA, USA

25 ⁷ Sandler Asthma Basic Research Center, University of California, San Francisco, CA, USA

26 ⁸Department of Experimental Medicine, University of California, San Francisco, CA, USA

27 ⁹ Genentech, Inc. San Francisco, CA, USA.
28 ¹⁰ Department of Gastroenterology, University of California, San Francisco, CA, USA
29 ¹¹ Benioff Center for Microbiome Medicine, University of California, San Francisco, CA, USA
30 ¹² Department of Pathology, University of California, San Francisco, CA, USA
31 ¹³ Lung Biology Center, University of California, San Francisco, CA, USA
32 ¹⁴ UCSF CoLabs, University of California, San Francisco, CA, USA
33 [†]COMET (COVID-19 Multiphenotyping for Effective Therapies) Consortium members are listed
34 in the Supplementary Appendix.

35

36

37 *Corresponding author

38 Email: chaz.langelier@ucsf.edu

39

40 **Keywords:** COVID-19, SARS-CoV-2, secondary bacterial pneumonia, VAP, metagenomics,
41 scRNA-seq

42

43 **Abstract**

44 Secondary bacterial infections, including ventilator-associated pneumonia (VAP), lead to
45 worse clinical outcomes and increased mortality following viral respiratory infections including in
46 patients with coronavirus disease 2019 (COVID-19). Using a combination of tracheal aspirate
47 bulk and single-cell RNA sequencing (scRNA-seq) we assessed lower respiratory tract immune
48 responses and microbiome dynamics in 28 COVID-19 patients, 15 of whom developed VAP, and
49 eight critically ill uninfected controls. Two days before VAP onset we observed a transcriptional
50 signature of bacterial infection. Two weeks prior to VAP onset, following intubation, we observed
51 a striking impairment in immune signaling in COVID-19 patients who developed VAP. Longitudinal
52 metatranscriptomic analysis revealed disruption of lung microbiome community composition in
53 patients with VAP, providing a connection between dysregulated immune signaling and outgrowth
54 of opportunistic pathogens. These findings suggest that COVID-19 patients who develop VAP
55 have impaired antibacterial immune defense detectable weeks before secondary infection onset.

56 **Introduction**

57 Secondary bacterial pneumonia results in significant morbidity and mortality in patients
58 with viral lower respiratory tract infections (LRTI)¹. This problem was evident in the 1918 influenza
59 pandemic during which the majority of deaths were ultimately attributed to secondary bacterial
60 pneumonia². SARS-CoV-2 infection, like influenza, confers an increased risk of late onset
61 secondary bacterial infection, often manifesting as ventilator-associated pneumonia (VAP)³.
62 Marked heterogeneity exists with respect to the risk of VAP in patients with coronavirus disease
63 2019 (COVID-19), with incidence ranging from 12-87% between published cohort studies⁴⁻⁷.

64 The mechanisms underlying VAP susceptibility in COVID-19 remain unknown, and no
65 biomarkers yet exist to inform risk of VAP at the time of intubation. Animal models of influenza
66 may provide some insight, suggesting a role for interferon-mediated suppression of cytokines
67 essential for bacterial defense, including neutrophil recruitment, antimicrobial peptide production
68 and the Th17 response⁸⁻¹⁰. Few human immunoprofiling studies have been conducted in VAP
69 however, and none have been reported in a prospective cohort of COVID-19 patients.

70 Lower respiratory infections represent a dynamic relationship between pathogen, host
71 response and the lung microbiome¹¹. Despite their interconnected roles, no studies to date have
72 simultaneously profiled host immune responses and lung microbiome dynamics in the context of
73 VAP. For instance, while prior work has described lung microbiome disruption in patients with
74 VAP^{11,12}, the question of whether host immune responses following viral infection may contribute
75 to this dysbiosis, leading to subsequent infection, remains unanswered.

76 Given the marked heterogeneity in VAP incidence among patients with COVID-19⁴⁻⁷, as
77 well as gaps in mechanistic understanding of secondary bacterial pneumonia, we sought to
78 assess the molecular determinants of VAP in the setting of SARS-CoV-2 infection. We employed
79 a systems biology approach involving immunoprofiling the host transcriptional response and
80 simultaneously assessing lung microbiome dynamics, using a combination of bulk and single cell
81 RNA sequencing and extensive clinical phenotyping. We observed a striking impairment in

82 antibacterial immune signaling at the time of intubation, that correlated with disruption of the lung
83 microbiome, weeks before the onset of VAP.

84

85 **Results**

86 We conducted a prospective case-control study of adults requiring mechanical ventilation
87 for COVID-19 or for illnesses other than pneumonia. Of 84 patients with COVID-19 initially
88 enrolled, tracheal aspirate (TA) specimens from 28 patients met inclusion criteria for analysis
89 (**Methods, Figure 1**). In addition, eight critically ill patients from a second cohort (Study 2,
90 **Methods**) were included as controls. Patients were enrolled at one tertiary care hospital and one
91 safety net hospital in San Francisco, California under research protocols approved by the
92 University of California San Francisco Institutional Review Board (**Methods**). We collected TA
93 periodically following intubation and performed bulk and scRNA-seq (**Methods**).

94 Patients with VAP were adjudicated using the United States Centers for Disease Control
95 (CDC) definition¹³, including a requirement for a positive bacterial TA culture (N=10). Patients who
96 met CDC VAP criteria but had negative bacterial TA cultures were only included in a secondary
97 analysis (N=5). We defined onset of VAP as the first day a patient developed any of the criteria
98 used to meet the definition, in accordance with CDC guidance. Patients who did not meet the
99 CDC-NHSN criteria for VAP, and for whom there was no sustained clinical suspicion for bacterial
100 pneumonia during the admission, were adjudicated as No-VAP (N=13).

101 We compared lower respiratory tract host transcriptional responses between the VAP and
102 No-VAP groups at two time points. “Early” time point TA samples were collected a median of two
103 days post-intubation and 17 days before VAP onset (bulk RNA-seq analysis) or nine days before
104 VAP onset (scRNA-seq). “Late” time point samples were collected a median of two days before
105 VAP onset for both bulk and scRNA-seq analyses and compared against samples collected from
106 No-VAP patients at similar timepoints post-intubation (**Figure 1, Table S1, Table S2**). We
107 additionally evaluated eight intubated patients with non-pneumonia illnesses as controls at the

108 “early” time-point. There were no significant differences between groups with respect to age,
109 gender, race or ethnicity (**Table S1, S2**). In addition, there were no differences between groups
110 with respect to in-hospital receipt of any immunosuppressant or antibiotics prior to sample
111 collection (**Table S3**).

112

113 **COVID-19 VAP is associated with a transcriptional signature of bacterial infection two days
114 before VAP onset**

115 We began by assessing the lower respiratory host transcriptional response two days
116 preceding VAP onset in COVID-19 patients. Differential gene expression analysis was carried out
117 on TA bulk RNA-seq data from five patients who developed VAP (samples collected a median of
118 two days before VAP onset) and eight patients who did not develop VAP collected within a similar
119 time frame after intubation (**Table S1**). We identified 436 differentially expressed genes at a False
120 Discovery Rate (FDR) < 0.1 (**Figure 2A**) and performed gene set enrichment analysis (GSEA)
121 (**Figure 2B**). The patients who developed VAP exhibited upregulation of pathways related to anti-
122 bacterial immune responses, such as neutrophil degranulation, toll-like receptor signaling,
123 cytokine signaling, and antigen presentation (**Figure 2B**). Interferon alpha/beta signaling was the
124 most upregulated pathway, suggesting prolonged viral infection in patients with VAP. Ingenuity
125 pathway analysis (IPA) additionally predicted broad activation of upstream inflammatory cytokines
126 in patients who developed VAP, in particular IFN α and IFN γ (**Figure 2C**).

127

128 **COVID-19 patients who develop VAP have attenuated immune signaling two weeks before
129 VAP onset**

130 Given our findings of a unique lower respiratory host transcriptional signature in the 48
131 hours preceding VAP onset, we next asked whether differences in host immune signaling might
132 exist even earlier, two or more weeks before clinical diagnosis of VAP, and whether such
133 differences might explain the increased susceptibility to secondary bacterial infection in these

134 patients. We thus compared TA gene expression soon after the time of intubation between
135 patients who eventually developed VAP (samples collected a median of two days post-intubation,
136 17 days before VAP onset, n= 4) and patients who did not develop VAP (samples collected a
137 median of two days after intubation, n = 8) (**Table 1**). We identified 154 differentially expressed
138 genes at FDR <0.1. The COVID-19 patients who developed VAP had lower expression of several
139 genes with roles in innate immunity including *IFI30*, *MMP2*, *TLR9*, and *DEFB124* (**Figure 3A**).
140 GSEA further revealed that patients who developed VAP had lower expression of pathways
141 related to antibacterial immune responses including neutrophil degranulation, toll-like receptor
142 signaling, IL-17 signaling, antigen presentation and complement pathways and higher expression
143 of IFN-alpha/beta signaling pathways, more than two weeks before the onset of VAP (**Figure 3B**).
144 Additionally, pathways related to adaptive immunity such as T and B cell receptor signaling were
145 also downregulated in patients who subsequently developed VAP (**Figure 3B**).

146 To gauge the degree of immune signaling suppression compared to controls, we
147 performed a similar analysis on critically ill intubated patients without infection (**Figure 3C**).
148 Relative to the control group, multiple antibacterial immune pathways were downregulated in
149 COVID-19 patients, with the greatest attenuation in the VAP group (**Figure 3C**). Upstream
150 regulator analysis identified impaired activation of diverse cytokines in those with VAP, while
151 *IFNB1* was notably upregulated (**Figure 3D**). Several pro-inflammatory cytokines were
152 downregulated in both groups compared to the controls (**Figure S1**). We expanded the
153 comparison at the “early” time-point to include patients with culture-negative VAP (VAP: n=6, No-
154 VAP: n=11) and observed similar differences at the pathway level (**Figure S2**).

155 Given prior reports demonstrating correlation between SARS-CoV-2 viral load and
156 interferon related gene expression¹⁴ we next asked whether viral load differed between VAP and
157 No-VAP patients. No differences in SARS-CoV-2 qPCR or viral reads per million (rpM) in bulk
158 RNA-seq data were found in the days following intubation (P = 0.84 (RNA-seq), P = 0.53 (PCR),
159 **Figure S3**). We also considered the possibility that differences in the number of days of steroid

160 exposure prior to sample collection might explain results, but found no differences ($P = 0.343$)
161 (**Table S1**).

162

163 **COVID-19 VAP is associated with impaired anti-bacterial immune signaling in monocytes,**
164 **macrophages and neutrophils**

165 To further understand the mechanism of early downregulation of key pathways involved
166 in antibacterial responses, we next asked whether this was driven by any one local immune cell
167 type. We performed scRNA-seq on TA specimens obtained early during disease course (median
168 of nine days before VAP) and enriched for immune cells using CD45 selection (**Methods**).
169 Clustering based upon cellular transcriptional signatures indicated that monocytes, macrophages
170 and neutrophils were the most abundant cell types (**Figure 4A, S4A**) and thus we focused
171 transcriptional assessment on these populations. A comparison of cell type proportions did not
172 reveal statistically significant differences in populations of mono/macs, neutrophils or T cells in
173 COVID-19 patients who subsequently developed VAP (**Figure 4B**).

174 COVID-19 patients who developed VAP had distinct cell type-specific transcriptional
175 signatures compared to those without VAP at this “early” post-intubation time-point (**Figure 4, S5,**
176 **S6**). With respect to mono/macs and neutrophils, we identified 532 and 693 differential expressed
177 genes, respectively, at $FDR < 0.05$. Several genes with key roles in innate immunity were
178 downregulated in both cell types in the COVID-19 patients who subsequently developed VAP
179 versus those who did not, including *IL1Rn*, *ICAM1*, *NFKB2*, and *ITGAX* in neutrophils, as well as
180 the neutrophil chemokines *CXCL2* and *CXCL8* in mono/macs (**Figure 4C, 4F, S5**). In addition,
181 similar to the bulk RNA-seq results demonstrating upregulation of type I IFN signaling at this time-
182 point in patients who developed VAP, we noted upregulation of several interferon-induced genes
183 including *IFI27* and *IFI30* in mono/macs, and *IFI30*, *IFITM1*, and *IFITM3* in neutrophils (**Figure**
184 **4C, F**).

185 IPA canonical pathway analysis of gene expression within each cluster revealed
186 downregulation of several cytokine and innate immune signaling pathways in the patients who
187 later developed VAP at the “early” post-intubation time-point. In the mono/mac cluster, this
188 included downregulation of IL-1, IL-6, and iNOS signaling, as well as Th17 and TNFR2 signaling
189 (**Figure 4D**). Analysis of the neutrophil cluster also demonstrated attenuated IL-1, IL-6, and
190 TNFR2 signaling and NF- κ B pathways (**Figure 4G**). COVID-19 patients who subsequently
191 developed VAP demonstrated upregulation of oxidative phosphorylation and glutathione
192 detoxification in the mono/mac subset, and interferon signaling, oxidative phosphorylation and
193 EIF2 signaling in the neutrophil cluster. Computational prediction of upstream cytokine activation
194 by IPA revealed impaired activation of multiple pro-inflammatory cytokines in both the mono/mac
195 and neutrophils in patients who developed VAP, including TNF, CXCL8, and IL1B, as well as
196 downregulation of key factors important in monocyte to macrophage differentiation (CSF2, CSF3,
197 *PF4*) (**Figure 4E, H**).

198 In the T cell population, we identified 1318 differentially expressed genes at FDR < 0.05.
199 Genes associated with T cell recruitment, including *CXCR6*, *ITGA1* and *ITGA4*, which have been
200 shown to regulate localization and retention of T cells in the lung during viral infection^{15,16}, were
201 downregulated in patients with VAP. Additionally, genes indicative of T cell activation (*CD69*,
202 *CD96*, *LAG3*, *ICOS*, *CD27*), signaling (*CD3*, *ZAP70*, *ITK*, *CD8A*, *CD8B*), and effector functions
203 (*IFNG*, *GZMA*, *GZMB*, *KLRG1*) were significantly downregulated in patients with VAP, suggesting
204 an impairment in T cell responses (**Figure S6A**). IPA revealed downregulation of signaling
205 pathways crucial for T cell recruitment, such as integrin signaling, and activation, such as *CD28*
206 signaling in helper T cells and phospholipase C signaling (**Figure S6B**).

207

208 **Temporal dynamics of the host response in COVID-19 patients who develop VAP**

209 We next investigated temporal dynamics of the lower airway host inflammatory response
210 in COVID-19 patients from the time of intubation to development of VAP by evaluating differential

211 gene expression between COVID-19 VAP patients at the “early” time point (median of 17 days
212 before VAP onset, n=4) versus “late” time point (median of two days before VAP onset, n=5) by
213 bulk RNA-seq. We identified 2705 differentially expressed genes (FDR<0.1) and unsupervised
214 hierarchical clustering of the 50 most significant genes demonstrated clear separation of the two
215 time-points (**Figure 5A**). GSEA revealed that type I interferon signaling was notably
216 downregulated at the “late” time-point most immediately preceding VAP onset in comparison to
217 the “early” timepoint (**Figure 5B**); however, expression was still significantly higher than in the
218 No-VAP patients (**Figure 2B**). Several other immune signaling pathways were more highly
219 expressed at this “late” time-point, presumably reflecting activation of an antibacterial response
220 in the setting of bacterial pneumonia (**Figure 5B**). Consistent with this, upstream regulator
221 analysis indicated increased activation of several pro-inflammatory cytokines and decreased
222 IFN α and IFN- λ signaling at the “late” versus “early” time-points (**Figure 5C**).

223 In contrast, comparing No-VAP patients at the “early” (n=8) versus “late” (n=8) time-points
224 yielded only two genes with a padj <0.1, both of which were interferon-stimulated genes (*RSAD2*
225 and *CMPK2*) downregulated at the “late” time-point, suggesting that while the host response was
226 relatively unchanged in these patients, the antiviral response attenuated over time. Indeed, GSEA
227 revealed that type I interferon signaling, and other antiviral immune pathways were downregulated
228 in the patients who did not develop VAP at the later time-point (**Figure S7**).

229 Next, we performed a similar comparison between the “early” and “late” time-points based
230 on scRNA-seq data from patients who developed VAP. Differential gene expression analysis on
231 these two populations identified 1368 differentially expressed genes (FDR<0.05) in the mono/mac
232 cluster, and 1028 in the neutrophil cluster. IPA revealed upregulation of antibacterial signaling
233 pathways at the later time-point, including signaling by several cytokines in the mono/mac cluster
234 (IL-17, IL-6, IL-1, TNF, IL-23, IFN) (**Figure 5D-E**), congruent with the bulk RNA-seq analysis.
235 Furthermore, we identified 1397 differentially expressed genes (FDR < 0.05) in the T cell cluster
236 between the two time-points and noted upregulation of signaling pathways indicative of an active

237 T cell response¹⁷ (e.g. ERK/MAPK, Tec kinase, and phospholipase C) in the days preceding VAP,
238 which was also in agreement with the bulk RNA-seq results (**Figure S6C**).

239 We further assessed dynamics of host immune responses between VAP and No-VAP
240 patients by performing longitudinal analyses of key immune signaling pathways, including all
241 patients with available TA samples (VAP n=7, No-VAP n=10). Onset of VAP in these patients
242 ranged from 10-39 days post intubation, with a median of 25 days, and treatment with
243 immunosuppressants did not differ significantly between VAP and no-VAP patients (p=0.304,
244 Fisher's exact test). We calculated pathway Z-scores for each sample by averaging Z-scores for
245 the top 20 leading edge genes of each pathway (**Methods**). Early attenuation of immune signaling
246 in the VAP group was conspicuous, and this pattern eventually resolved later in disease course
247 by the time secondary bacterial infection became established (**Figures 5E-H**). We confirmed that
248 the observed differences between VAP and no-VAP patients were not driven by differences in
249 treatment with immunosuppressants by comparing pathway Z-scores in patients that received
250 immunosuppressants and those that did not at the early time-point regardless of VAP group
251 (**Figure S8**).

252

253 **Lung microbiome disruption precedes VAP in COVID-19 patients**

254 We hypothesized that the innate immune suppression in patients who developed VAP
255 would correlate with viral load. Using TA metatranscriptomics to assess the lower respiratory
256 microbiome, we evaluated longitudinal changes in SARS-CoV-2 abundance. Although no
257 difference was observed at the “early” timepoint (**Figure S3**), the trajectory of SARS-CoV-2 viral
258 load differed significantly in patients who developed VAP (p=0.0058), although in both groups
259 decreased over time (**Figure 6A**). This result suggested that COVID-19 patients who develop
260 VAP may exhibit impaired ability to clear virus compared to those who do not, and that the lung
261 microbiome composition may be similarly impacted.

Indeed, COVID-19 patients who developed VAP exhibited a significant reduction in bacterial diversity of their airway microbiome up to three weeks before clinical signs of infection (Shannon Diversity Index, $p=0.012$; **Figure 6B**). COVID-19 patients who developed VAP also had lower airway microbiome compositions more closely resembling each other than those from patients who did not develop VAP, across all timepoints since intubation (Bray Curtis index, $p=0.0033$; **Figure 6C**), suggesting community collapse precedes the development of VAP. All patients received antibiotics prior to collection of the first sample, suggesting that antibiotic use was not driving these differences (**Table S1**).

270

271 Discussion

Secondary bacterial pneumonia contributes to significant morbidity and mortality in patients with primary viral lower respiratory tract infections^{1,3}, but mechanisms governing individual susceptibility to VAP have remained unclear. Few human cohort studies have evaluated the immunologic underpinnings of VAP, and none have been reported in the context of COVID-19, which is characterized by a dysregulated host response distinct from other viral pneumonias^{14,18,19}. To address this gap and probe mechanisms of VAP susceptibility in patients with COVID-19, we carried out a systems biological assessment of host and microbial dynamics of the lower respiratory tract.

Two days before VAP onset, a transcriptional signature consistent with bacterial infection was observed. This finding suggests that host response changes can occur before clinical recognition of pneumonia, highlighting the potential utility of the host transcriptome as a tool for VAP surveillance. While intriguing, this observation did not provide an explanation for differential susceptibility of some COVID-19 patients to post-viral pneumonia.

The discovery of an early suppressed antibacterial immune response in patients who later developed VAP did however, offer a potential explanation. More than two weeks before VAP onset, we observed a striking suppression of pathways related to both innate and adaptive

288 immunity, including neutrophil degranulation, TLR signaling, complement activation, antigen
289 presentation, and T cell receptor and B receptor signaling, as well as cytokine signaling (e.g. IL-
290 1, IL-4, IL-12, IL-13 and IL-17). Comparison against uninfected, intubated controls confirmed the
291 previously described paradoxical impairment in immune signaling found in patients with severe
292 COVID-19¹⁸, and suggested that VAP susceptibility may be the result of disproportionate
293 suppression of innate and adaptive pathways critical for antibacterial defense, resulting in
294 enhanced susceptibility to opportunistic secondary infections.

295 Animal models of influenza have provided insight into potential mechanisms of post-viral
296 pneumonia, although none have provided insight regarding why some individuals are more
297 susceptible than others. In mice inoculated with influenza, for instance, virus-induced type I IFN
298 suppresses neutrophil chemokines and impairs Th17 immunity, compromising effective clearance
299 of bacterial infections^{9,10}. Interestingly, we also observed increased type I interferon signaling in
300 COVID-19 patients who weeks later developed VAP, and a strikingly similar impairment in Th17
301 signaling and other immune pathways. Desensitization to toll-like receptor (TLR) ligands after
302 influenza infection has also been documented²⁰, which is congruent with the downregulation of
303 TLR signaling at the time of intubation observed in our bulk RNA-seq analyses.

304 Impaired bacterial clearance by alveolar macrophages was found to be driven by virus-
305 related IFN γ production by T cells²¹ in a murine post-influenza model. In contrast, we found that
306 T cells from patients who later developed VAP expressed lower levels of IFN γ at the time of
307 intubation. This difference may relate to species-specific variations in immune signaling or intrinsic
308 differences in the host response to influenza virus versus SARS-CoV-2^{14,18}.

309 We asked whether certain cell types were responsible for driving the early suppression of
310 immune signaling observed in COVID-19 patients who went on to develop VAP. No significant
311 differences in proportions of the most abundant cell types - monocytes/macrophages, neutrophils
312 or T cells – was observed between patients with or without VAP at the time of intubation. This

313 finding suggests that an impairment of immune cell recruitment was not causing these differences,
314 but rather significant gene expression differences within each of these immune cell populations.

315 In both the mono/mac and neutrophil populations, we observed broad downregulation of
316 the innate immune response, and initiation of the adaptive immune response, concordant with
317 global observations in bulk RNA-seq analyses. Further analysis revealed a downregulation of
318 monocyte to macrophage differentiation and neutrophil chemotaxis. Further, we noted a
319 downregulation of key pathways and transcription factors involved in antimicrobial immune
320 responses including iNOS in mono/macs, as well as NFKB and TREM1 in mono/macs and
321 neutrophils. Both bulk and scRNA-seq suggested an impairment in T cell recruitment, signaling,
322 and effector functions. Overall, our data suggest that while no difference in cell type populations
323 existed between groups, changes in the gene expression of mono/macs, neutrophils and T cells
324 contributes to immune suppression in COVID-19 patients who later develop VAP.

325 SARS-CoV-2 viral load correlates with interferon stimulated gene expression^{14,18} and thus
326 we initially hypothesized that differences in viral load between groups might relate to individual
327 VAP susceptibility. However, we found no difference between groups at the “early” timepoint.
328 Moreover, no differences existed in terms of immunosuppressive medication administration or
329 clinically diagnosed immunodeficiency, suggesting that other, still unidentified mechanisms
330 present at the time of intubation must underlie the marked suppression of immune gene
331 expression in COVID-19 patients who went on to develop VAP.

332 While no difference in viral load was observed at the time of intubation, the COVID-19
333 patients who developed VAP exhibited impaired viral clearance over the time-course of intubation.
334 This observation was corroborated by a prolonged antiviral type I interferon response at the “late”
335 timepoint (median of two days before VAP onset) in patients who developed VAP versus those
336 who did not, pointing to the persistence of suboptimal antiviral immunity in these patients. Early
337 induction of functional SARS-CoV-2 specific T cells is associated with faster viral clearance in

338 COVID-19 patients²² and likewise, we observed impairments in T cell activation and signaling in
339 the VAP group, which further suggests a decreased ability to control the virus in these patients.

340 Respiratory viruses can reshape the human airway microbiome by modulating host
341 inflammatory responses^{23,24}. In mouse models of influenza, the airway microbiome exhibits
342 expansion of several bacterial families during the course of viral infection as innate immunity is
343 suppressed²³. These changes increase the risk of secondary bacterial infection²³ and have been
344 observed in patients with chronic obstructive pulmonary disease, where suppression of the innate
345 immune response in rhinovirus infected patients may be followed by bacterial superinfection^{25,26}.

346 Similarly, the innate immune suppression observed in COVID-19 patients who developed
347 VAP was associated with airway microbiome collapse and the outgrowth of lung pathogens in
348 advance of clinical VAP diagnosis. This finding suggests that individual immune responses to
349 SARS-CoV-2 infection may drive a restructuring of the microbial community and increase
350 susceptibility to VAP (**Figure 7**). The resulting outgrowth of a VAP-associated bacterial pathogen
351 may elicit an antibacterial response, but the broader immunosuppressive state preceding this
352 response may be insufficient to control the development of clinical pneumonia. Those with a
353 lesser degree of immunosuppression may be able to respond faster and therefore control
354 opportunistic bacterial pathogens more effectively.

355 These findings may also have important implications for management of patients with
356 COVID-19 related acute respiratory failure, many of whom are now being treated with
357 corticosteroids plus/minus IL-6 receptor blocking agents. These agents may lead to further
358 suppression of the key pathways required for host response to secondary bacterial infection.
359 Thus, our results emphasize the need for ongoing vigilance for VAP in patients treated with potent
360 immunosuppressive agents, as well as the need to develop novel diagnostic and/or prognostic
361 approaches to identifying patients at highest risk. For instance, availability of molecular
362 biomarkers to assess a patient's risk of VAP at the time of intubation could reduce inappropriate
363 use of prophylactic antibiotics or immunomodulatory treatments, or signal a need for enhanced

364 surveillance strategies. Signatures of immune dysfunction have been used as biomarkers to
365 predict nosocomial infection in critically ill patients,²⁷ although not in the context of viral infection.

366 Sample size is a limitation of this study; however, the reproducibility of our observations
367 across both bulk and scRNA-seq analyses and the significant number of differentially expressed
368 genes among the comparator groups support the validity of our conclusions. Because this study
369 was limited to critically ill, intubated patients, we were unable to assess early stages of COVID-
370 19, which may provide additional insight regarding determinants of secondary bacterial infection.
371 Additionally, we were unable to assess whether epithelial cells contributed to VAP risk due to
372 enrichment for immune cells prior to scRNA-seq. With larger cohorts, the early detection of
373 specific immune pathway suppression and microbiome collapse could be leveraged to develop
374 clinically useful models for identifying COVID-19 patients with increased susceptibility to
375 secondary bacterial pneumonia.

376

377 **Materials and Methods**

378

379 **Study design, cohorts, enrollment and ethics approval**

380 We conducted a prospective case-control study of adults requiring mechanical ventilation
381 for COVID-19 with or without secondary bacterial pneumonia. We also evaluated control patients
382 requiring mechanical ventilation for other reasons who had no evidence of pulmonary infection
383 (**Figure 1**). Patients were enrolled in either of two prospective cohort studies of critically ill patients
384 at the University of California, San Francisco (UCSF) and Zuckerberg San Francisco General
385 Hospital between 07/2013 and 07/2020. Both cohort studies were approved by the UCSF
386 Institutional Review Board (IRB) under protocols 10-02701 (control patients, pre-COVID-19
387 pandemic) and 20-30497 (COVID-19 patients, COVID-19 Multiphenotyping for Effective Therapy
388 (COMET) study), respectively. Of the COVID-19 patients, 19 were co-enrolled in the National

389 Institute of Allergy and Infectious Diseases-funded Immunophenotyping Assessment in a COVID-
390 19 Cohort (IMPACC) Network study.

391 For both the COVID-19 and control cohorts, if a patient met inclusion criteria, then a study
392 coordinator or physician obtained written informed consent for enrollment from the patient or their
393 surrogate. Patients or their surrogates were provided with detailed written and verbal information
394 about the goals of the study, the data and specimens that would be collected, and the potential
395 risks to the subject. Patients and their surrogates were also informed that there would be no
396 benefit to them from being enrolled in the study and that they may withdraw informed consent at
397 any time during the course of the study. All questions were answered, and informed consent
398 documented by obtaining the signature of the patient or their surrogate on the consent document
399 (or during the COVID-19 pandemic, the IRB-approved electronic equivalent, to enable touchless
400 consent).

401 Many critically ill patients are unconscious at the time of intensive care unit (ICU)
402 admission due to their underlying illness and/or are endotracheally intubated for airway
403 management or acute respiratory failure. The patients who are not unconscious are often in pain
404 and may have acute delirium due to critical illness and/or medications. For these reasons, many
405 subjects are unable to provide informed consent at the time of enrollment. Because this study
406 could not practically be done otherwise and was deemed to be minimal risk by the UCSF IRB, if
407 a patient was unable and a surrogate was not available to provide consent, patients were enrolled
408 with waiver of initial consent, including the collection of biological samples.

409 Specifically, for subjects who were unable to provide informed consent at the time of
410 enrollment, our study team was permitted to collect biological samples as well as clinical data
411 from the medical record obtained prior to consent. Surrogate consent was vigorously pursued for
412 all patients; moreover, each patient was regularly examined to determine if and when s/he was
413 able to consent for him/herself, and the nursing and ICU staff were contacted daily for information

414 about surrogates' availability. For patients whose surrogates provided informed consent, follow-
415 up consent was subsequently obtained from the patient if they survived their acute illness and
416 regained the ability to consent. For subjects who died prior to the consent being obtained, a full
417 waiver of consent was approved by the UCSF IRB for both cohort studies. Lack of a surrogate to
418 provide consent is common in critically ill patients. To address this, the UCSF IRB also approved
419 a full waiver of consent for subjects in the COVID-19 cohort who remained unable to provide
420 informed consent and had no contactable surrogate identified within 28 days. Before utilizing this
421 waiver, we made and documented at least three separate attempts to identify and contact the
422 patient or surrogate over a month-long period. While most patients enrolled were consented by
423 typical processes, three died prior to consent being obtained, and five were included with a full
424 waiver of consent due to lack of ability to consent and lack of contactable surrogate. No personally
425 identifiable information has been included as part of this manuscript for any enrolled patients.

426

427 **Ventilator-associated pneumonia adjudication**

428 A total of 84 adults who required intubation for severe COVID-19 (Cohort 1) and who had
429 available TA samples were considered for inclusion in the study (**Figure 1**). Patients who met the
430 Centers for Disease Control (CDC) definition for VAP¹³ with a positive bacterial sputum culture
431 were adjudicated as having VAP for the purpose of the study (N=16); patients who did not meet
432 these criteria, and for whom there was no sustained clinical suspicion for bacterial pneumonia
433 during the admission, were categorized as No-VAP (N=17). VAP and No-VAP patients for whom
434 samples at the time-points of interest were available were included in the primary analyses (VAP:
435 N=10; No-VAP: N=13). Patients who met CDC-VAP criteria but had negative TA cultures were
436 included in a secondary supplementary analysis only (N=5). All other patients were excluded,
437 including patients with clinically-suspected bacterial pneumonia who did not meet CDC VAP
438 criteria. Eight intubated patients from a recent study¹⁸ (Cohort 2) were included as controls and

439 were selected because they had previously been adjudicated as having no evidence of lower
440 respiratory tract infection. This group included four patients with the acute respiratory distress
441 syndrome (ARDS) due to non-infectious etiologies, and four patients without ARDS who were
442 intubated for other reasons (subdural hematoma (N=1), retroperitoneal hemorrhage (N=1), or
443 neurosurgical procedures (N=2)).

444

445 **Tracheal aspirate sampling**

446 Following enrollment, tracheal aspirate (TA) was collected (periodically following
447 intubation for Study 1, or once within 3 days of intubation for Study 2), without addition of saline
448 wash, and either a) mixed 1:1 with DNA/RNA shield (Zymo Research) for bulk RNA-seq or b)
449 immediately processed in a biosafety level 3 laboratory (BSL3) for scRNA-seq analysis.

450

451 **Bulk RNA sequencing and host transcriptome analysis**

452

453 RNA sequencing

454 To evaluate host and microbial gene expression, metatranscriptomic next generation RNA
455 sequencing (RNA-seq) was performed on TA specimens. Following RNA extraction (Zymo
456 Pathogen Magbead Kit) and DNase treatment, human cytosolic and mitochondrial ribosomal RNA
457 was depleted using FastSelect (Qiagen). To control for background contamination, we included
458 negative controls (water and HeLa cell RNA) as well as positive controls (spike-in RNA standards
459 from the External RNA Controls Consortium (ERCC))²⁸. RNA was then fragmented and
460 underwent library preparation using the NEBNext Ultra II RNA-seq Kit (New England BioLabs).
461 Libraries underwent 146 nucleotide paired-end Illumina sequencing on an Illumina Novaseq 6000.
462

463 Host differential expression

464 Following demultiplexing, sequencing reads were pseudo-aligned with kallisto²⁹ to an
465 index consisting of all transcripts associated with human protein coding genes (ENSEMBL v.
466 99), cytosolic and mitochondrial ribosomal RNA sequences and the sequences of ERCC RNA
467 standards. Gene-level counts were generated from the transcript-level abundance estimates
468 using the R package tximport³⁰, with the scaledTPM method. Samples retained in the dataset
469 had a total of at least 1,000,000 estimated counts associated with transcripts of protein coding
470 genes.

471 Genes were retained for differential expression analysis if they had counts in at least 30%
472 of samples. Differential expression analysis was performed using the R package DESeq2³¹. We
473 modeled the expression of individual genes using the design formula ~VAPgroup, where VAP
474 groups were “VAP-early”, “No VAP-early”, “VAP-late” and “No VAP-late” and used the results()
475 function to extract a specific contrast. Separate comparisons to the control group were performed
476 using the design formula ~COVID-19-status to compare positive and negative patients.

477 Significant genes were identified using a Benjamini-Hochberg false discovery rate (FDR)
478 < 0.1. We generated heatmaps of the top 50 differentially expressed genes by FDR. For
479 visualization, gene expression was normalized using the regularized log transformation, centered,
480 and scaled prior to clustering. Heatmaps were generated using the *pheatmap* package. Columns
481 were clustered using Euclidean distance and rows were clustered using Pearson correlation.
482 Differential expression analysis results are provided in (**Supplementary data file 1**).

483

484 Pathway analysis

485 Gene set enrichment analyses (GSEA) were performed using the fgseaMultilevel function
486 in the R package fgsea³² and REACTOME pathways³³ with a minimum size of 10 genes and a
487 maximum size of 1,500 genes. All genes were included in the comparison, pre-ranked by the test
488 statistic. Significant pathways were defined as those with a Benjamini-Hochberg adjusted p-value

489 < 0.05. Ingenuity Pathway Analysis (IPA) Canonical Pathway and Upstream Regulator Analysis³⁴
490 was employed on genes with p<0.1 and ranked by the test statistic to identify cytokine regulators.
491 Significant IPA results were defined as those with a Z-score absolute value greater than 2 and an
492 overlap P value < 0.05. The gene sets in figures were selected to reduce redundancy and highlight
493 diverse biological functions. Full GSEA and IPA results are provided in (**Supplementary data**
494 **files 2 and 3**).

495 Longitudinal pathway analysis was performed using all available TA samples spanning
496 post-intubation to VAP onset for all patients included in the bulk RNA-seq analysis. Analysis was
497 restricted to samples with at least 1,000,000 human protein coding transcripts. Pathways of
498 interest were selected from the significant GSEA results of the comparison of VAP vs. No-VAP
499 patients in the “early” time-point. The top 20 leading edge genes were selected from each pathway
500 for analysis. To calculate a Z-score for each gene, expression was normalized using the variance
501 stabilizing transformation (VST), centered, and scaled. A pathway Z-score was calculated by
502 averaging the 20 gene Z-scores. Multiple Z-scores per patient at a given time interval were
503 averaged so that each patient corresponds to one datapoint at each interval. Statistical
504 significance of pathway expression over time between VAP and No-VAP groups was calculated
505 using a two-way analysis of variance (ANOVA) in GraphPad PRISM.

506

507 **Single cell RNA sequencing and transcriptome analysis**

508 After collection, fresh TA was transported to a BSL-3 laboratory at ambient temperature
509 to improve neutrophil survival. 3mL of TA was dissociated in 40mL of PBS with 50ug/mL
510 collagenase type 4 (Worthington) and 0.56 ku/mL of Dnase I (Worthington) for 10 minutes at room
511 temperature, followed by passage through a 70µM filter. Cells were pelleted at 350g 4C for 10
512 minutes, resuspended in PBS with 2mM EDTA and 0.5% BSA, and manually counted on a
513 hemocytometer. Cells were stained with MojoSort Human CD45 and purified by the
514 manufacturer’s protocol (Biolegend). After CD45 positive selection, cells were manually counted

515 with trypan blue on a hemocytometer. Using a V(D)J v1.1 kit according to the manufacturer's
516 protocol, samples were loaded on a 10X Genomics Chip A without multiplexing, aiming to capture
517 10,000 cells (10X Genomics). Libraries underwent paired end 150 base pair sequencing on an
518 Illumina NovaSeq6000.

519 Raw sequencing reads were aligned to GRCh38 using the STAR aligner³⁵. Cell barcodes
520 were then determined based upon UMI count distribution. Read count matrices were generated
521 through the 10X genomics cellranger pipeline v3.0. Data was processed and analyzed using the
522 Scanpy v1.6³⁶. Cells that had <200 genes and had greater than 30,000 counts were filtered.
523 Mitochondrial genes were removed and multi-sample integration was performed using Harmony
524 v0.1.4³⁷. Differential expression was performed using MAST v1.16.0³⁸. Due to the significantly
525 greater number of differentially expressed genes in scRNA-seq analyses, we used a more
526 restrictive cutoff of FDR < 0.05 for significant genes. Differential expression analysis results are
527 detailed in (**Supplementary data file 4**).

528

529 Pathway analysis

530 Ingenuity Pathway Analysis (IPA) Canonical Pathway and Upstream Regulator Analysis³⁴
531 was employed on genes with p<0.05 and ranked by log2foldchange to identify canonical pathways
532 and cytokine regulators. We utilized a more restrictive p value cutoff for scRNA-seq to ensure a
533 similar number of genes were input into IPA. Significant IPA results were defined as those with a
534 Z-score absolute value greater than 2 and an overlap P value < 0.05. The gene sets in figures
535 were selected to reduce redundancy and highlight diverse biological functions. Full GSEA and
536 IPA results are provided in (**Supplementary data files 5 and 6**).

537

538 **Lung microbiome analysis**

539 RNA from tracheal aspirates was sequenced as described above. Taxonomic alignments
540 were obtained from raw sequencing reads using the IDseq pipeline^{39,40}, which performs quality

541 filtration and removal of human reads followed by reference-based taxonomic alignment at both
542 the nucleotide and amino acid level against sequences in the National Center for Biotechnology
543 Information (NCBI) nucleotide (NT) and non-redundant (NR) databases, followed by assembly of
544 reads matching each taxon detected. Taxonomic alignments underwent background correction
545 for environmental contaminants (see below), viruses were excluded, and data was then
546 aggregated to the genus level before calculating diversity metrics. Alpha diversity (Shannon's
547 Diversity Index) and beta diversity (Bray-Curtis dissimilarity) were calculated and the latter plotted
548 using non-metric multidimensional scaling (NDMS). Comparison of alpha and beta diversity over
549 time between VAP and No-VAP groups was calculated using a two-way analysis of variance
550 (ANOVA) in GraphPad PRISM.

551

552 Identification and mitigation of environmental contaminants

553 To minimize inaccurate taxonomic assignments due to environmental and reagent derived
554 contaminants, non-templated “water only” and HeLa cell RNA controls were processed with each
555 group of samples that underwent nucleic acid extraction. These were included, as well as positive
556 control clinical samples, with each sequencing run. Negative control samples enabled estimation
557 of the number of background reads expected for each taxon. A previously developed negative
558 binomial model¹⁴ was employed to identify taxa with NT sequencing alignments present at an
559 abundance significantly greater compared to negative water controls. This was done by modeling
560 the number of background reads as a negative binomial distribution, with mean and dispersion
561 fitted on the negative controls. For each batch (sequencing run) and taxon, we estimated the
562 mean parameter of the negative binomial by averaging the read counts across all negative
563 controls, slightly regularizing this estimate by including the global average (across all batches) as
564 an additional sample. We estimated a single dispersion parameter across all taxa and batches,
565 using the functions `glm.nb()` and `theta.md()` from the R package MASS⁴¹. Taxa that achieved a p-
566 value <0.01 were carried forward.

567 **References**

- 568 1. Falsey, A. R. et al. Bacterial Complications of Respiratory Tract Viral Illness: A
569 Comprehensive Evaluation. *The Journal of Infectious Diseases* **208**, 432–441 (2013).
- 570 2. Morens, D. M., Taubenberger, J. K. & Fauci, A. S. Predominant role of bacterial pneumonia
571 as a cause of death in pandemic influenza: implications for pandemic influenza
572 preparedness. *J Infect Dis* **198**, 962–970 (2008).
- 573 3. Rouzé, A. et al. Relationship between SARS-CoV-2 infection and the incidence of ventilator-
574 associated lower respiratory tract infections: a European multicenter cohort study. *Intensive
575 Care Med* 1–11 (2021) doi:10.1007/s00134-020-06323-9.
- 576 4. Luyt, C.-E. et al. Ventilator-associated pneumonia in patients with SARS-CoV-2-associated
577 acute respiratory distress syndrome requiring ECMO: a retrospective cohort study. *Ann
578 Intensive Care* **10**, 158 (2020).
- 579 5. Bardi, T. et al. Nosocomial infections associated to COVID-19 in the intensive care unit:
580 clinical characteristics and outcome. *Eur J Clin Microbiol Infect Dis* (2021)
581 doi:10.1007/s10096-020-04142-w.
- 582 6. Maes, M. et al. Ventilator-associated pneumonia in critically ill patients with COVID-19. *Crit
583 Care* **25**, 25 (2021).
- 584 7. Søgaard, K. K. et al. Community-acquired and hospital-acquired respiratory tract infection
585 and bloodstream infection in patients hospitalized with COVID-19 pneumonia. *J Intensive
586 Care* **9**, (2021).
- 587 8. Metzger, D. W. & Sun, K. Immune Dysfunction and Bacterial Co-Infections following
588 Influenza. *J Immunol* **191**, 2047–2052 (2013).
- 589 9. Shahangian, A. et al. Type I IFNs mediate development of postinfluenza bacterial pneumonia
590 in mice. *J Clin Invest* **119**, 1910–1920 (2009).
- 591 10. Kudva, A. et al. Influenza A inhibits Th17-mediated host defense against bacterial
592 pneumonia in mice. *J Immunol* **186**, 1666–1674 (2011).

- 593 11. Langelier, C. *et al.* Integrating host response and unbiased microbe detection for lower
594 respiratory tract infection diagnosis in critically ill adults. *Proc Natl Acad Sci U S A* **115**,
595 E12353–E12362 (2018).
- 596 12. Flanagan, J. L. *et al.* Loss of bacterial diversity during antibiotic treatment of intubated
597 patients colonized with *Pseudomonas aeruginosa*. *J Clin Microbiol* **45**, 1954–1962 (2007).
- 598 13. CDC-NHSN. Pneumonia (Ventilator-associated [VAP] and non-ventilator-associated
599 Pneumonia [PNEU]) Event.
- 600 14. Mick, E. *et al.* Upper airway gene expression reveals suppressed immune responses to
601 SARS-CoV-2 compared with other respiratory viruses. *Nature Communications* **11**, 5854
602 (2020).
- 603 15. Wein, A. N. *et al.* CXCR6 regulates localization of tissue-resident memory CD8 T cells to the
604 airways. *Journal of Experimental Medicine* **216**, 2748–2762 (2019).
- 605 16. Grau, M. *et al.* Antigen-Induced but Not Innate Memory CD8 T Cells Express NKG2D and
606 Are Recruited to the Lung Parenchyma upon Viral Infection. *The Journal of Immunology*
607 **200**, 3635–3646 (2018).
- 608 17. Smith-Garvin, J. E., Koretzky, G. A. & Jordan, M. S. T cell activation. *Annu Rev Immunol* **27**,
609 591–619 (2009).
- 610 18. Sarma, A. *et al.* COVID-19 ARDS is characterized by a dysregulated host response that
611 differs from cytokine storm and is modified by dexamethasone. *Res Sq* (2021)
612 doi:10.21203/rs.3.rs-141578/v1.
- 613 19. Blanco-Melo, Daniel. Imbalanced host response to SARS-CoV-2 drives development of
614 COVID-19. *Cell*. doi:10.1016/j.cell.2020.04.026.
- 615 20. Didierlaurent, A. *et al.* Sustained desensitization to bacterial Toll-like receptor ligands after
616 resolution of respiratory influenza infection. *J Exp Med* **205**, 323–329 (2008).
- 617 21. Sun, K. & Metzger, D. W. Inhibition of pulmonary antibacterial defense by interferon-gamma
618 during recovery from influenza infection. *Nat Med* **14**, 558–564 (2008).

- 619 22. Tan, A. T. *et al.* Early induction of functional SARS-CoV-2-specific T cells associates with
620 rapid viral clearance and mild disease in COVID-19 patients. *Cell Reports* **34**, 108728
621 (2021).
- 622 23. Goulding, J. *et al.* Lowering the Threshold of Lung Innate Immune Cell Activation Alters
623 Susceptibility to Secondary Bacterial Superinfection. *J Infect Dis* **204**, 1086–1094 (2011).
- 624 24. Man, W. H., de Steenhuijsen Piters, W. A. A. & Bogaert, D. The microbiota of the respiratory
625 tract: gatekeeper to respiratory health. *Nat Rev Microbiol* **15**, 259–270 (2017).
- 626 25. Mallia, P. *et al.* Rhinovirus Infection Induces Degradation of Antimicrobial Peptides and
627 Secondary Bacterial Infection in Chronic Obstructive Pulmonary Disease. *Am J Respir Crit
628 Care Med* **186**, 1117–1124 (2012).
- 629 26. Molyneaux, P. L. *et al.* Outgrowth of the Bacterial Airway Microbiome after Rhinovirus
630 Exacerbation of Chronic Obstructive Pulmonary Disease. *Am J Respir Crit Care Med* **188**,
631 1224–1231 (2013).
- 632 27. Conway Morris, A. *et al.* Cell-surface signatures of immune dysfunction risk-stratify critically
633 ill patients: INFECT study. *Intensive Care Med* **44**, 627–635 (2018).
- 634 28. Pine, P. S. *et al.* Evaluation of the External RNA Controls Consortium (ERCC) reference
635 material using a modified Latin square design. *BMC Biotechnol* **16**, 54 (2016).
- 636 29. Bray, N. L., Pimentel, H., Melsted, P. & Pachter, L. Near-optimal probabilistic RNA-seq
637 quantification. *Nature Biotechnology* **34**, 525–527 (2016).
- 638 30. Soneson, C., Love, M. I. & Robinson, M. D. Differential analyses for RNA-seq: transcript-
639 level estimates improve gene-level inferences. *F1000Res* **4**, 1521 (2015).
- 640 31. Love, M. I., Huber, W. & Anders, S. Moderated estimation of fold change and dispersion for
641 RNA-seq data with DESeq2. *Genome Biol* **15**, 550 (2014).
- 642 32. Korotkevich, G., Sukhov, V. & Sergushichev, A. Fast gene set enrichment analysis. *bioRxiv*
643 060012 (2019) doi:10.1101/060012.

- 644 33. Croft, D. *et al.* The Reactome pathway knowledgebase. *Nucleic Acids Res* **42**, D472-477
645 (2014).
- 646 34. Krämer, A., Green, J., Pollard, J. & Tugendreich, S. Causal analysis approaches in
647 Ingenuity Pathway Analysis. *Bioinformatics* **30**, 523–530 (2014).
- 648 35. Dobin, A. *et al.* STAR: ultrafast universal RNA-seq aligner. *Bioinformatics* **29**, 15–21 (2013).
- 649 36. Wolf, F. A., Angerer, P. & Theis, F. J. SCANPY : large-scale single-cell gene expression
650 data analysis. *Genome Biology* **19**, 15 (2018).
- 651 37. Korsunsky, I. *et al.* Fast, sensitive, and accurate integration of single cell data with
652 Harmony. *bioRxiv* 461954 (2018) doi:10.1101/461954.
- 653 38. Finak, G. *et al.* MAST: a flexible statistical framework for assessing transcriptional changes
654 and characterizing heterogeneity in single-cell RNA sequencing data. *Genome Biol* **16**, 278
655 (2015).
- 656 39. Ramesh, A. *et al.* Metagenomic next-generation sequencing of samples from pediatric
657 febrile illness in Tororo, Uganda. *PLoS One* **14**, e0218318 (2019).
- 658 40. Kalantar, K. L. *et al.* IDseq—An open source cloud-based pipeline and analysis service for
659 metagenomic pathogen detection and monitoring. *Gigascience* **9**, (2020).
- 660 41. Venables, W. N. & Ripley, B. D. *Modern Applied Statistics with S*. (Springer-Verlag, 2002).
661 doi:10.1007/978-0-387-21706-2.
- 662
- 663
- 664
- 665

666 Acknowledgements: This study was performed with support from the National Institute of Allergy
667 and Infectious Diseases-sponsored Immunophenotyping Assessment in a COVID-19 Cohort
668 (IMPACC) Network. We gratefully appreciate support from Amy Kistler, PhD, Jack Kamm, PhD,
669 Angela Deitweiller, PhD, Saharai Caldera, BS and Maira Phelps BS.

670

671 Funding: Funding for the COMET cohort enrollment, sample collection and data analysis derived
672 from: K23HL138461-01A1 (CL), K24HL137013 (PGW), F32 HL151117 (AS), R35 HL140026
673 (CSC), NIAID U19AI077439 (DJE), Chan Zuckerberg Biohub (AB, JLD). The UCSF IMPACC site
674 was funded by NIAID U19AI077439 (DJE). Funding for enrollment of COMET participants not
675 enrolled in IMPACC and for all sample collection and data analysis derived from K23HL138461-
676 01A1 (CL), K24HL137013 (PGW), F32 HL151117 (AS), R35 HL140026 (CSC), and the Chan
677 Zuckerberg Biohub (AB, JLD). Philanthropic support was provided from Mark and Carrie Casey,
678 Julia and Kevin Hartz, Carl Kawaja and Wendy Holcombe, Eric Keisman and Linda Nevin, Martin
679 and Leesa Romo, Three Sisters Foundation, Diana Wagner and Jerry Yang and Akiko Yamazaki.

680

681 Author contributions:

682 Conceptualization: CRL, AT, BSZ, AB, CD, SL, ER, OR, CSC

683 Methodology: CRL, AT, BSZ, AB, CD, SL, ER, OR

684 Data acquisition: RG, AJ, PHS, TJD, BSZ, AB, NJ

685 Formal analysis: AT, BSZ, AB, CD, SL, ER, EM

686 Investigation: BSZ, AB, CD, SS, CSC, DJE

687 Funding acquisition: CRL, CSC, JLD, DJE

688 Supervision: CRL, OR, NN, JLD, CSC, DJE

689 Writing - original draft: AT, BSZ, AB, CD, SL, ER, CRL

690 Writing - review & editing: All authors

691

692 Competing interests: Authors declare that they have no competing interests.

693

694 Materials and Correspondence: Correspondence and material requests should be addressed to

695 Chaz Langelier (chaz.langelier@ucsf.edu).

696

697 Data and materials availability: Host gene expression data are available under NCBI GEO

698 accession number GSE168019 for bulk RNA-seq and GSE168018 for scRNA-seq. Raw microbial

699 sequencing alignments are available from NCBI SRA under BioProject PRJNA704082. Code

700 used for differential expression analysis is available at <https://github.com/bspeco/VAPinCOVID19>

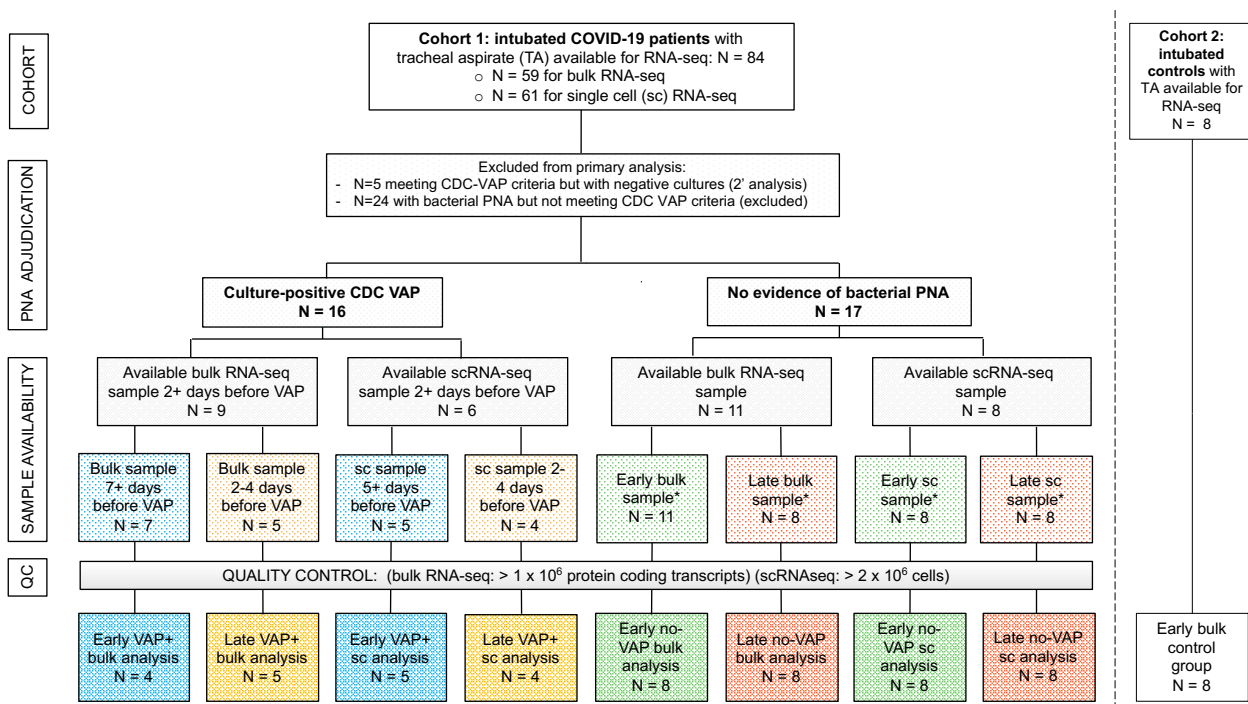


Figure 1: Study flowchart.

Two patient cohorts were studied. Cohort 1 consisted of COVID-19 patients from the COVID Multiphenotyping for Effective Therapies (COMET) / Immunophenotyping Assessment in a COVID-19 Cohort (IMPACC) studies (described in Methods). Cohort 2 consisted of critically ill intubated control patients from a prior prospective cohort study led by our research group¹⁸. The “early” samples were the first available tracheal aspirate specimens after intubation. For COVID-19 patients who developed VAP, the “late” samples were obtained a median of two days before VAP onset. Timing of sample collection with respect to VAP versus No-VAP groups was matched at “early” and “late” time points. Controls included eight critically ill, mechanically ventilated patients without LRTI. All COVID-19 patients included in the primary bulk analysis were also included in the longitudinal host expression and microbiome analyses. Abbreviations: VAP=ventilator-associated pneumonia; TA=tracheal aspirate; QC=quality control; sc or scRNA-seq= single cell RNA sequencing; PNA=pneumonia; CDC=United States Centers for Disease Control and Prevention.

Figure 2

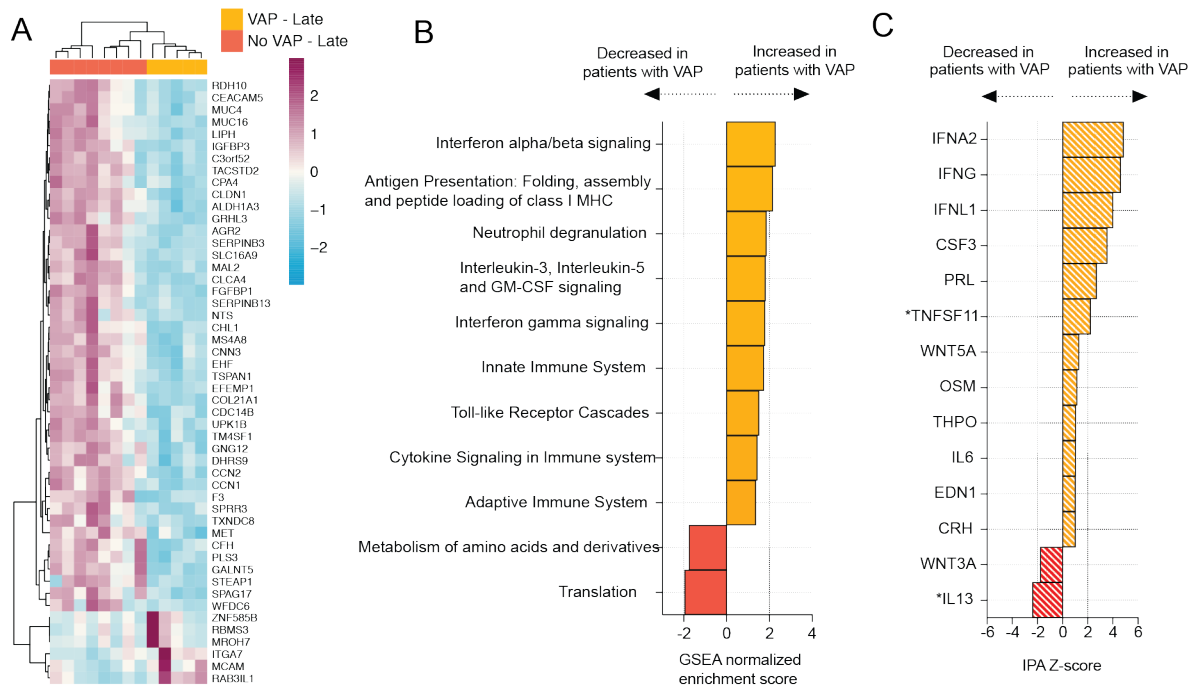


Figure 2: COVID-19 VAP is associated with a lower respiratory tract transcriptional signature of bacterial infection 2 days before VAP onset.

A) Heatmap of the top 50 differentially expressed genes by adjusted P-value between COVID-19 patients who developed VAP (yellow) versus those who did not (red) at the “late” time-point, 2 days before the onset of VAP, from bulk RNA-seq. **B)** Gene set enrichment analysis (GSEA) at the “late” time-point based on differential gene expression analyses. GSEA results were considered significant with an adjusted P-value <0.05 . **C)** Ingenuity Pathway Analysis (IPA) of upstream cytokines at the “late” time-point based on differential gene expression analyses. IPA results were considered significant with a Z-score absolute value >2 and overlap P-value <0.05 .

*Denotes cytokines with an overlap P-value < 0.1 . All pathways and cytokines are shown in Supplementary data files 2 and 3.

Figure 3

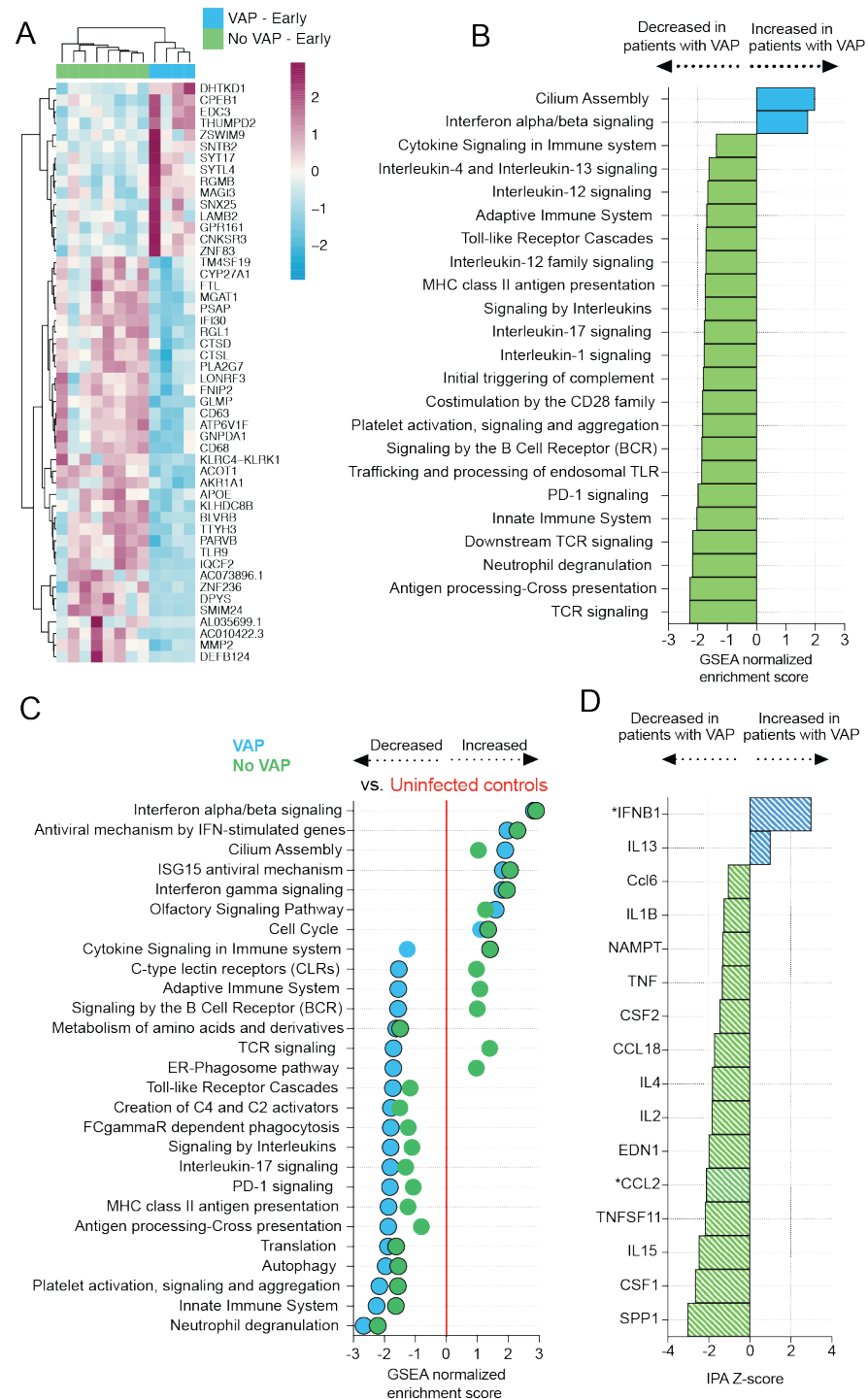


Figure 3: COVID-19 patients who develop VAP have attenuated immune signaling in the lower respiratory tract two weeks before onset of secondary bacterial pneumonia.

A) Heatmap of the top 50 differentially expressed genes by adjusted P-value between COVID-19 patients who developed VAP (blue) versus those who did not (green) at the “early” time-point from bulk RNA-seq. **B)** Gene set enrichment analysis at the “early” time-point based on differential gene expression analyses. GSEA results were considered significant with an adjusted P-value <0.05. **C)** Expression of GSEA pathways at the “early” time-point with respect to a baseline of uninfected, intubated controls. Pathways were selected from the GSEA results if they had an adjusted P-value <0.05 in at least one of the comparisons (VAP vs controls or No-VAP vs controls). Pathways with an adjusted P-value <0.05 when compared to controls are indicated by circles with a black outline. **D)** Ingenuity Pathway Analysis (IPA) of upstream cytokines at the “early” time-point based on differential gene expression analyses. IPA results were considered significant with a Z-score absolute value >2 and overlap P-value <0.05. *Denotes cytokines with an overlap P-value <0.1. All pathways and cytokines are shown in Supplementary data files 2 and 3.

Figure 4

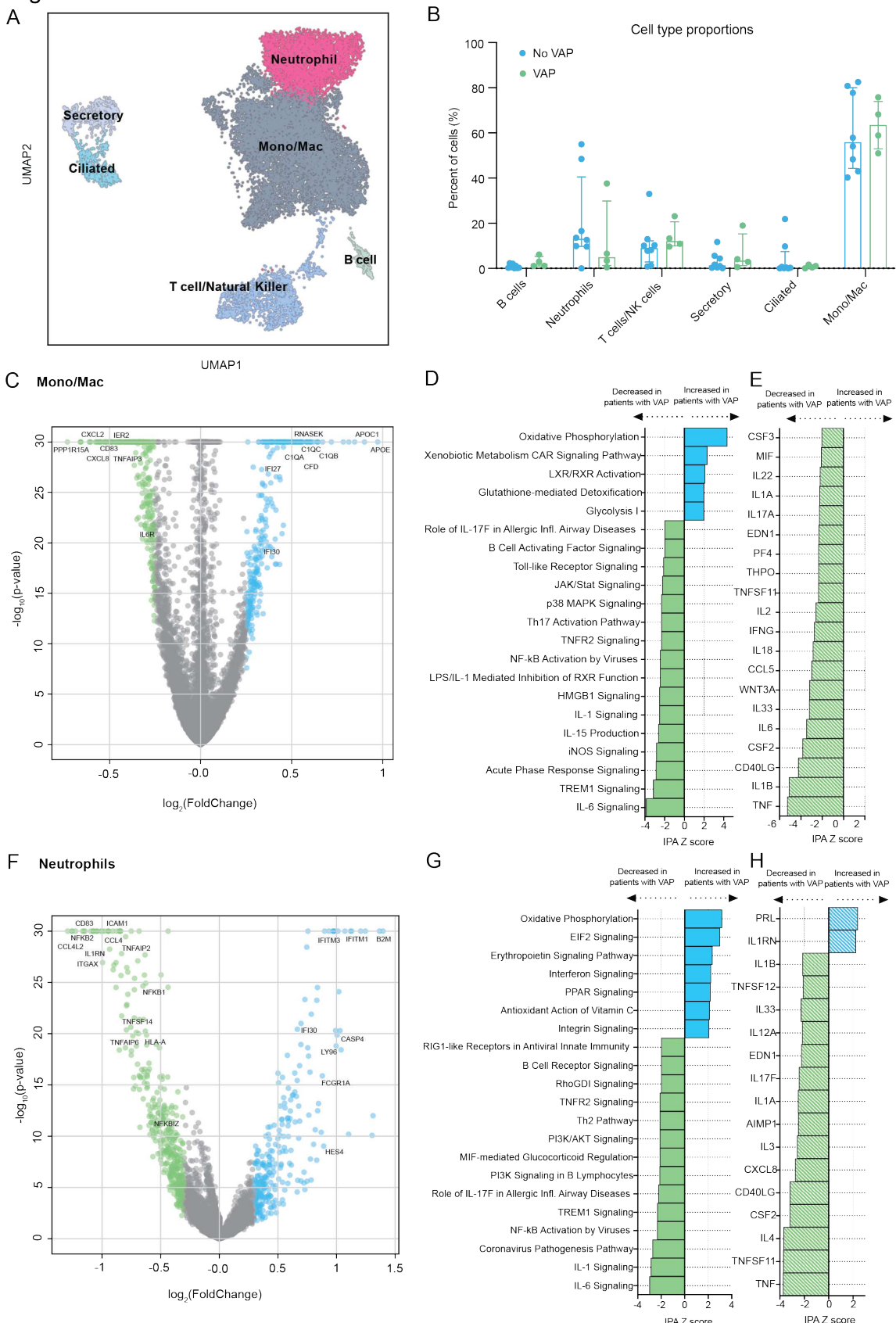


Figure 4: scRNA-seq demonstrates that COVID-19 VAP is associated with early impaired anti-bacterial immune signaling in lower respiratory tract monocytes, macrophages and neutrophils.

A) UMAP of single cell RNA-seq data from patients that do or do not develop VAP at the “early” time-point, annotated by cell type. **B)** Cell type proportions in single cell RNA-seq from VAP and No-VAP patients at the “early” time-point. Bars represent the median with IQR. Statistical significance was determined by Mann-Whitney tests. None of the cell types were significantly different with a p-value <0.05. The p-values for each cell type are as follows: B cells: 0.073; Neutrophils: 0.28; T/NK cells: 0.21; Secretory: 0.46; Ciliated: 0.94, and Mono/Mac: 0.81. **C)** Volcano plot displaying the differentially expressed genes between VAP and No-VAP patients in monocytes and macrophages. **D)** Ingenuity Pathway Analysis (IPA) of key canonical pathways and upstream cytokines based on differential gene expression analysis in monocytes and macrophages of patients who develop VAP versus those who do not, with adjusted p-values < 0.05. Only significant pathways (IPA Z-score of >2 or <-2 and overlap p-value <0.05) are shown. **E)** Volcano plot displaying the differentially expressed genes between VAP and No-VAP patients in neutrophils. **F)** IPA of canonical pathways and upstream cytokines based on differential gene expression analysis in neutrophils of patients who develop VAP versus those who do not, with adjusted p-values < 0.05. Only significant pathways (IPA Z-score of >2 or <-2 and overlap p-value <0.05) are shown. All pathways and cytokines are shown in Supplementary data files 5 and 6.

Figure 5

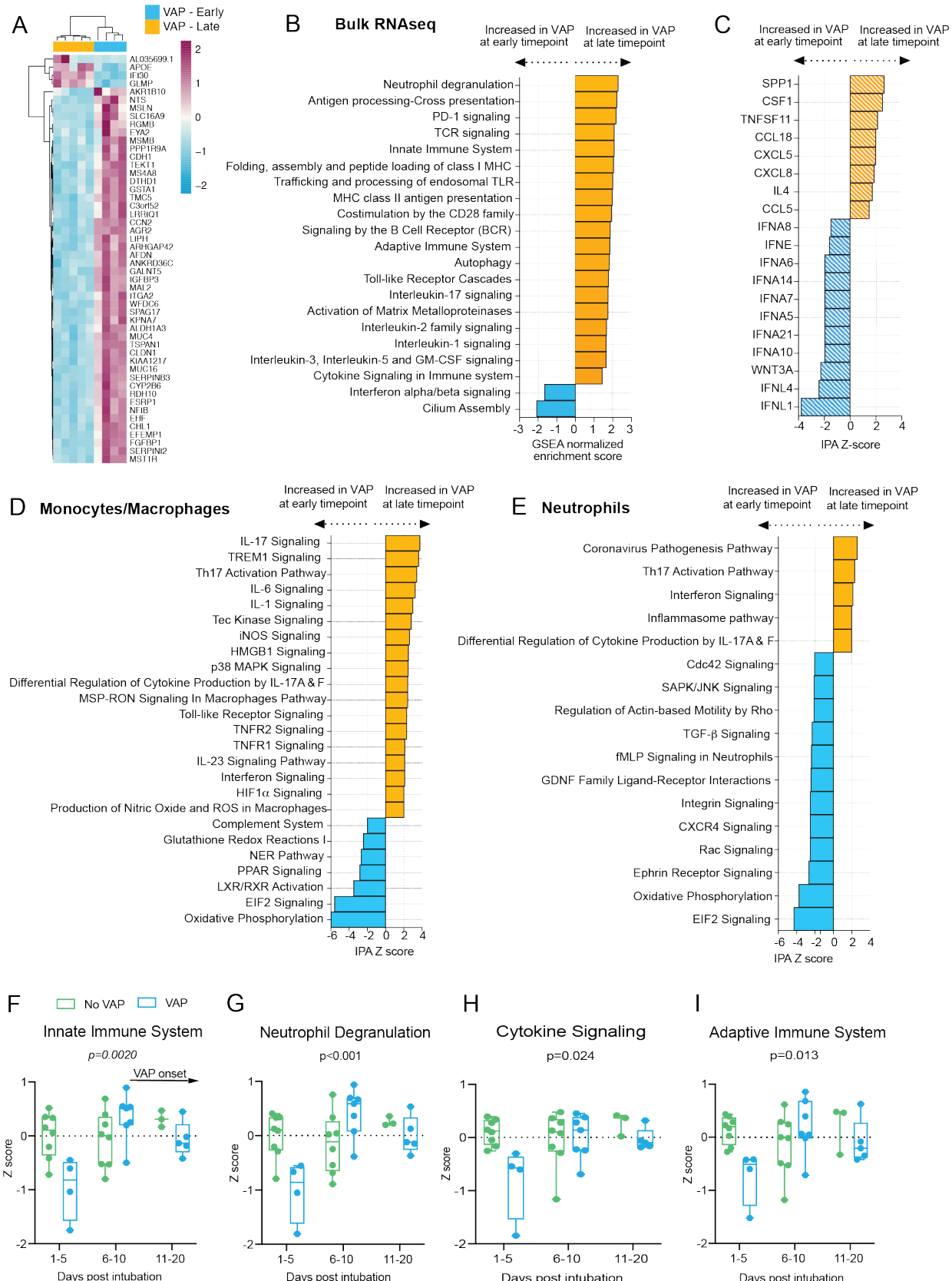


Figure 5: Temporal dynamics of the host response to VAP

A) Heatmap of the top 50 differentially expressed genes by adjusted P-value between COVID-19 patients who developed VAP at the “early” time-point (blue) versus the “late” time-point (yellow) from bulk RNA-seq. **B)** Gene set enrichment analysis (GSEA) based on differential gene expression of VAP patients at the “early” vs “late” time-point from bulk RNA-seq. GSEA results were considered significant with an adjusted P-value <0.05 . **C)** Ingenuity Pathway Analysis (IPA) of upstream cytokines based on differential gene expression analyses of VAP patients at the “early” vs “late” time-point from bulk RNA-seq. IPA results were considered significant with a Z-score absolute value >2 and overlap P-value <0.05 . **(D-E)** Ingenuity Pathway Analysis (IPA) of key canonical pathways based on differential gene expression analysis in monocytes and macrophages (D) or neutrophils (E) from scRNA-seq of patients who develop VAP versus those who do not, with adjusted p-values < 0.05 . Only significant pathways (IPA Z-score of >2 or <-2 and overlap p-value <0.05) are shown. All pathways and cytokines are shown in Supplementary data files 2, 3, 5, and 6. **(F-I)** Longitudinal analysis of selected pathway expression in VAP (blue) versus No-VAP (green) patients from bulk RNA-seq samples taken from time of intubation to onset of VAP for all patients. Pathway Z-scores were calculated by averaging Z-scores for the top 20 leading edge genes of each pathway, determined by the results of GSEA comparing VAP versus No-VAP patients at the “early” time-point. Multiple Z-scores per patient at a given time interval were averaged so that each patient corresponds to one datapoint at each interval. Samples from day 21+ after intubation are not shown due to a lack of these later time-points in the No-VAP group. VAP onset in these patients ranged from 10-39 days post intubation. Selected pathways are innate immune system (F), neutrophil degranulation (G), cytokine signaling (H), and adaptive immune system (I). Box plots represent the median and range. Statistical significance was determined by two-way ANOVA, and interaction p-values are shown.

Figure 6

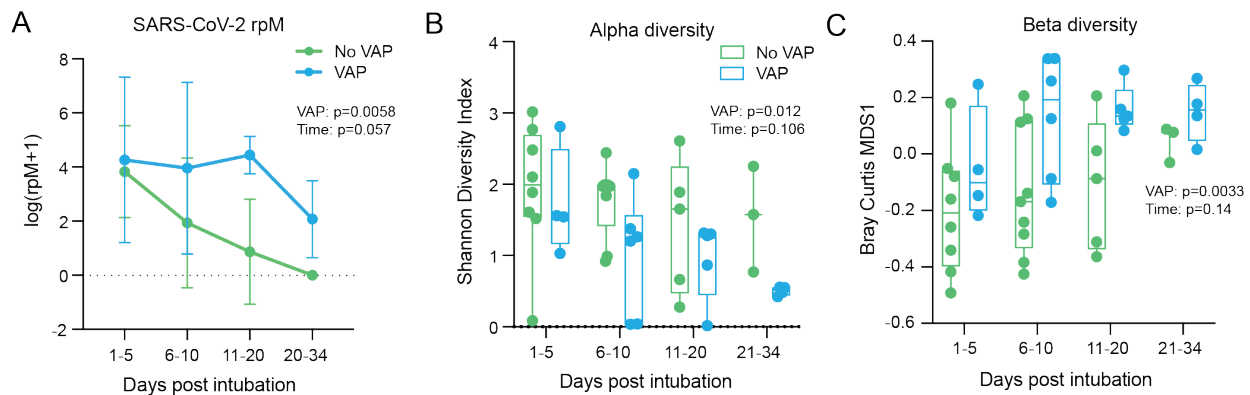


Figure 6: Lung microbiome community collapse precedes VAP in COVID-19 patients.

(A) SARS-CoV-2 viral load (reads per million sequenced, rpM) over time by days since intubation in patients who develop VAP vs those who do not. For plotting purposes, $\log(\text{rpM}+1)$ was used to avoid negative values. Lung microbiome (B) bacterial diversity (Shannon's Index) and (C) β -diversity (Bray Curtis Index, NMDS scaling) in COVID-19 patients with relation to VAP development over time by days since intubation. Box plots represent the median and range (A-C). Statistical significance was determined by two-way ANOVA. P-values <0.05 were considered significant.

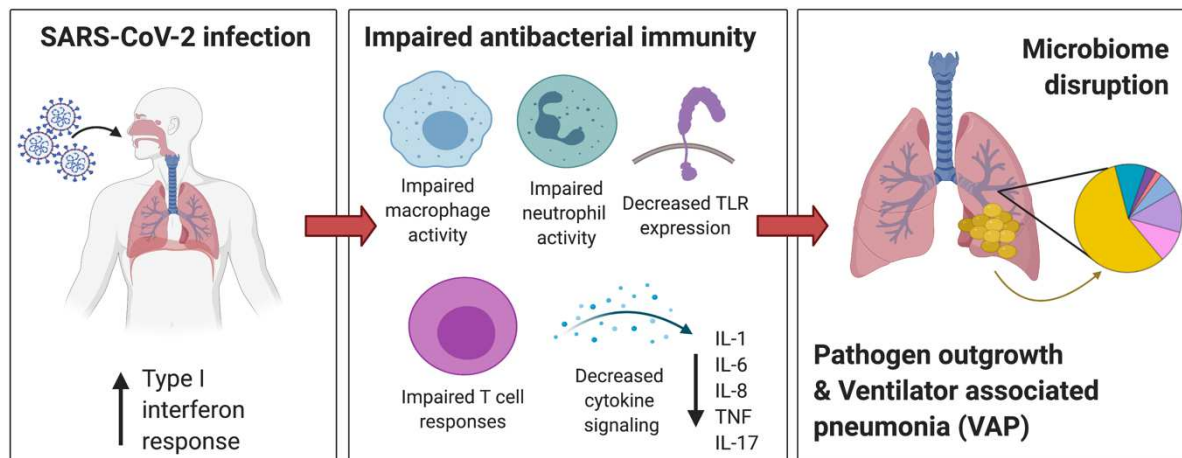


Figure 7: Mechanistic hypothesis of secondary bacterial pneumonia susceptibility in patients with COVID-19.

Individual immune responses to SARS-CoV-2 infection drive a restructuring of the microbial community and increase susceptibility to VAP. Those predisposed to VAP have increased type I interferon responses and dysregulated antibacterial immune signaling characterized by impaired macrophage, neutrophil and T cell activity, decreased TLR signaling and impaired activation of key cytokines important for pathogen defense including IL-1, IL-6, IL-8, TNF, and IL-17. This state of suppressed immunity disrupts the lower respiratory tract microbiome, predisposing to outgrowth of bacterial pathogens and VAP.

Figures

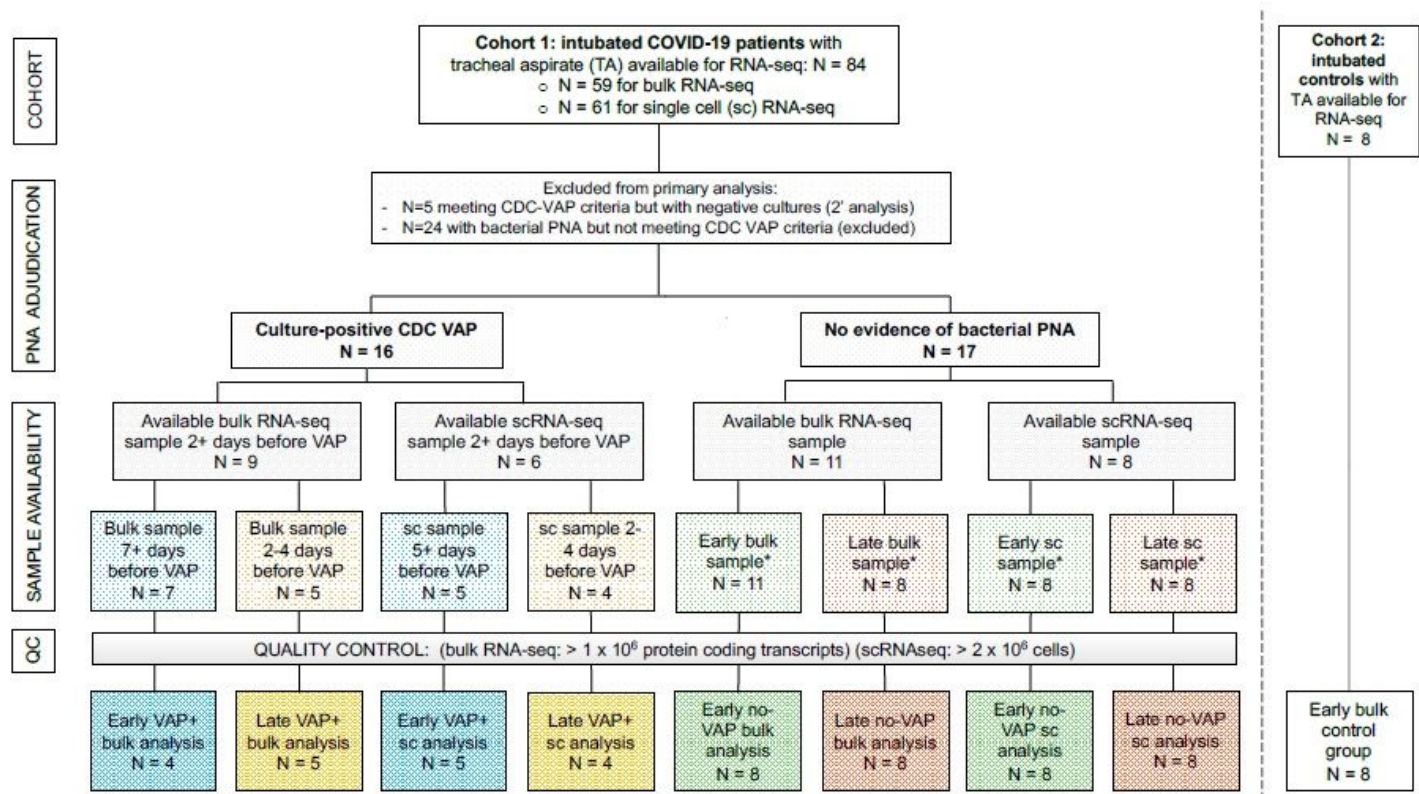


Figure 1

Study flowchart. Two patient cohorts were studied. Cohort 1 consisted of COVID-19 patients from the COVID Multiphenotyping for Effective Therapies (COMET) / Immunophenotyping Assessment in a COVID-19 Cohort (IMPACC) studies (described in Methods). Cohort 2 consisted of critically ill intubated control patients from a prior prospective cohort study led by our research group 18. The “early” samples were the first available tracheal aspirate specimens after intubation. For COVID-19 patients who developed VAP, the “late” samples were obtained a median of two days before VAP onset. Timing of sample collection with respect to VAP versus No-VAP groups was matched at “early” and “late” time points. Controls included eight critically ill, mechanically ventilated patients without LRTI. All COVID-19 patients included in the primary bulk analysis were also included in the longitudinal host expression and microbiome analyses. Abbreviations: VAP=ventilator-associated pneumonia; TA=tracheal aspirate; QC=quality control; sc or scRNAseq= single cell RNA sequencing; PNA=pneumonia; CDC=United States Centers for Disease Control and Prevention.

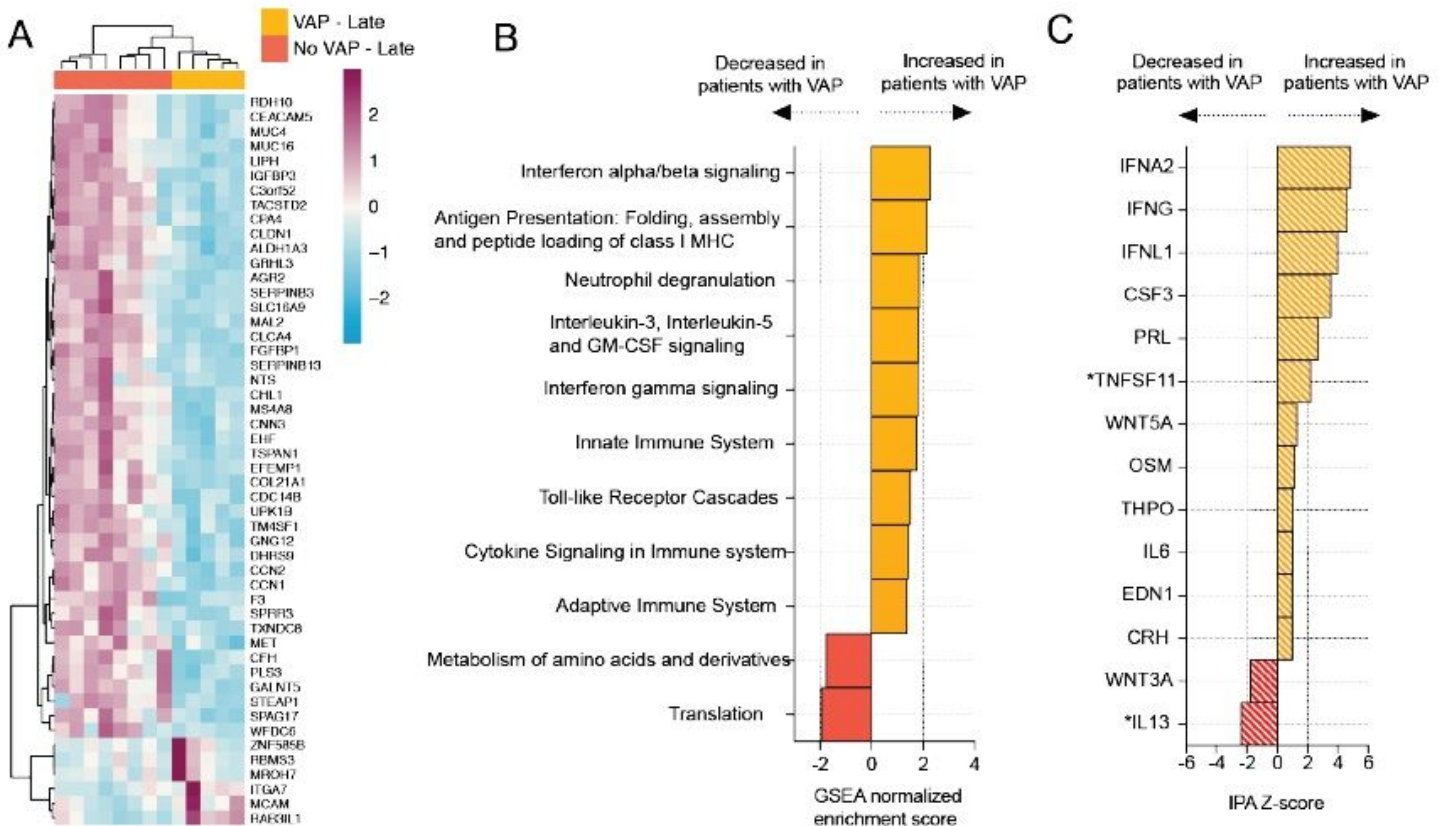


Figure 2

COVID-19 VAP is associated with a lower respiratory tract transcriptional signature of bacterial infection 2 days before VAP onset. A) Heatmap of the top 50 differentially expressed genes by adjusted P-value between COVID-19 patients who developed VAP (yellow) versus those who did not (red) at the "late" time-point, 2 days before the onset of VAP, from bulk RNA-seq. B) Gene set enrichment analysis (GSEA) at the "late" time-point based on differential gene expression analyses. GSEA results were considered significant with an adjusted P-value <0.05 . C) Ingenuity Pathway Analysis (IPA) of upstream cytokines at the "late" time-point based on differential gene expression analyses. IPA results were considered significant with a Z-score absolute value >2 and overlap P-value <0.05 . *Denotes cytokines with an overlap P-value < 0.1 . All pathways and cytokines are shown in Supplementary data files 2 and 3.

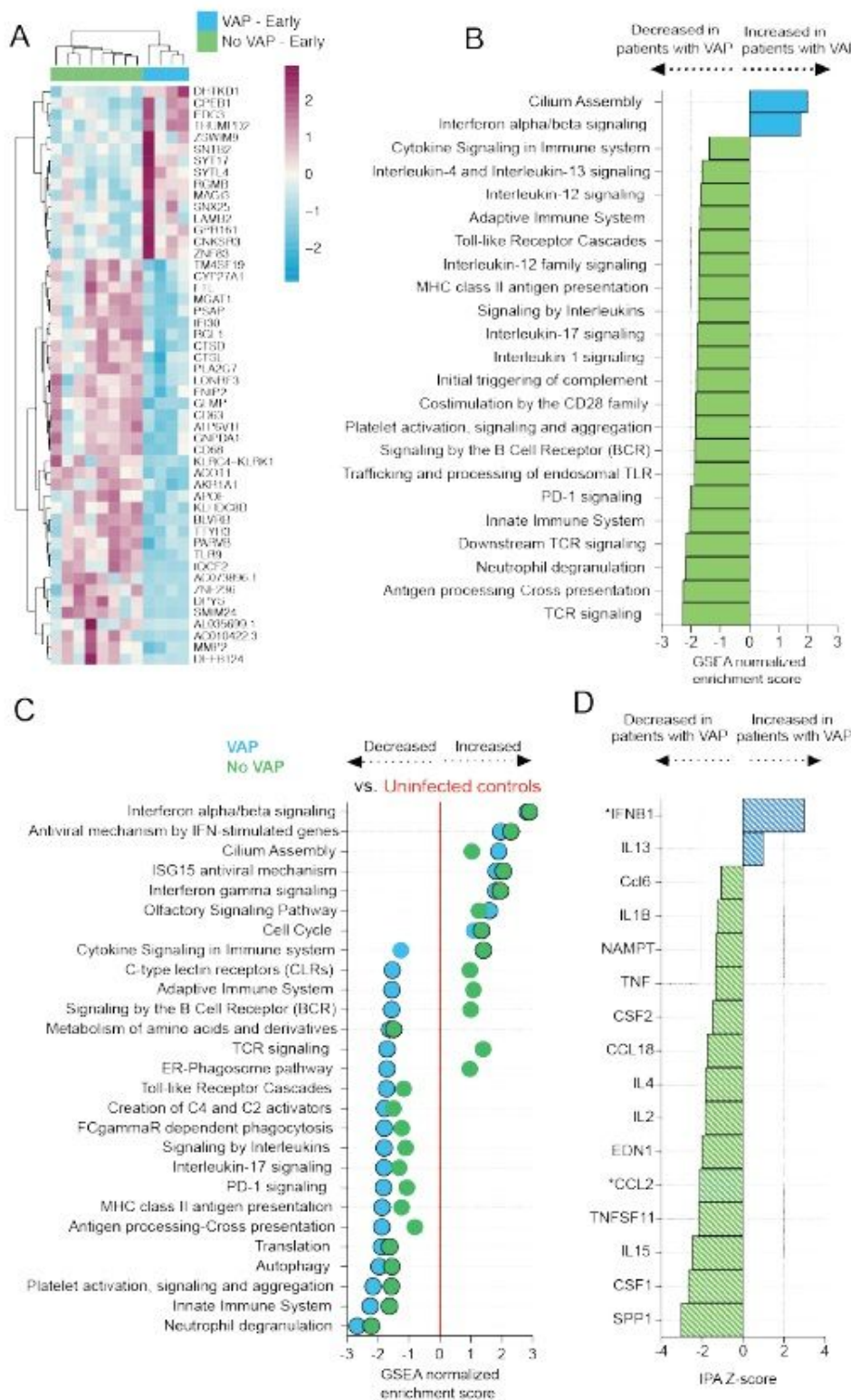


Figure 3

COVID-19 patients who develop VAP have attenuated immune signaling in the lower respiratory tract two weeks before onset of secondary bacterial pneumonia. A) Heatmap of the top 50 differentially expressed genes by adjusted P-value between COVID-19 patients who developed VAP (blue) versus those who did not (green) at the “early” time-point from bulk RNA-seq. B) Gene set enrichment analysis at the “early” time-point based on differential gene expression analyses. GSEA results were considered significant with

an adjusted P-value <0.05. C) Expression of GSEA pathways at the “early” time-point with respect to a baseline of uninfected, intubated controls. Pathways were selected from the GSEA results if they had an adjusted P-value <0.05 in at least one of the comparisons (VAP vs controls or No-VAP vs controls). Pathways with an adjusted P-value <0.05 when compared to controls are indicated by circles with a black outline. D) Ingenuity Pathway Analysis (IPA) of upstream cytokines at the “early” time-point based on differential gene expression analyses. IPA results were considered significant with a Z-score absolute value >2 and overlap P-value <0.05. *Denotes cytokines with an overlap P-value <0.1. All pathways and cytokines are shown in Supplementary data files 2 and 3.

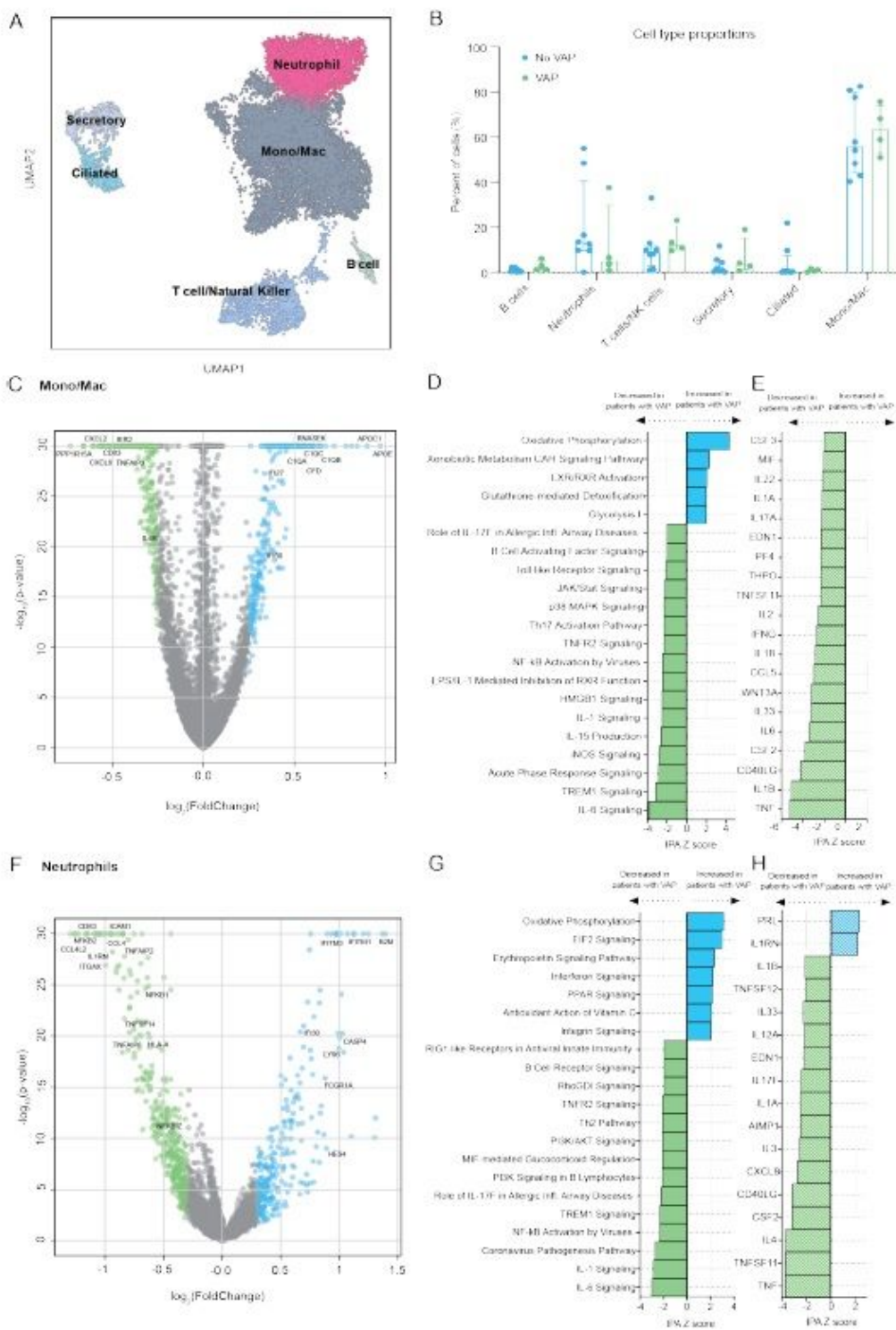


Figure 4

scRNA-seq demonstrates that COVID-19 VAP is associated with early impaired anti-bacterial immune signaling in lower respiratory tract monocytes, macrophages and neutrophils. A) UMAP of single cell RNA-seq data from patients that do or do not develop VAP at the “early” time-point, annotated by cell type. B) Cell type proportions in single cell RNA-seq from VAP and No-VAP patients at the “early” time-point. Bars represent the median with IQR. Statistical significance was determined by Mann-Whitney

tests. None of the cell types were significantly different with a p-value <0.05. The p-values for each cell type are as follows: B cells: 0.073; Neutrophils: 0.28; T/NK cells: 0.21; Secretory: 0.46; Ciliated: 0.94, and Mono/Mac: 0.81. C) Volcano plot displaying the differentially expressed genes between VAP and No-VAP patients in monocytes and macrophages. D) Ingenuity Pathway Analysis (IPA) of key canonical pathways and upstream cytokines based on differential gene expression analysis in monocytes and macrophages of patients who develop VAP versus those who do not, with adjusted p-values < 0.05. Only significant pathways (IPA Z-score of >2 or <-2 and overlap p-value <0.05) are shown. E) Volcano plot displaying the differentially expressed genes between VAP and No-VAP patients in neutrophils. F) IPA of canonical pathways and upstream cytokines based on differential gene expression analysis in neutrophils of patients who develop VAP versus those who do not, with adjusted p-values < 0.05. Only significant pathways (IPA Z-score of >2 or <-2 and overlap p-value <0.05) are shown. All pathways and cytokines are shown in Supplementary data files 5 and 6.

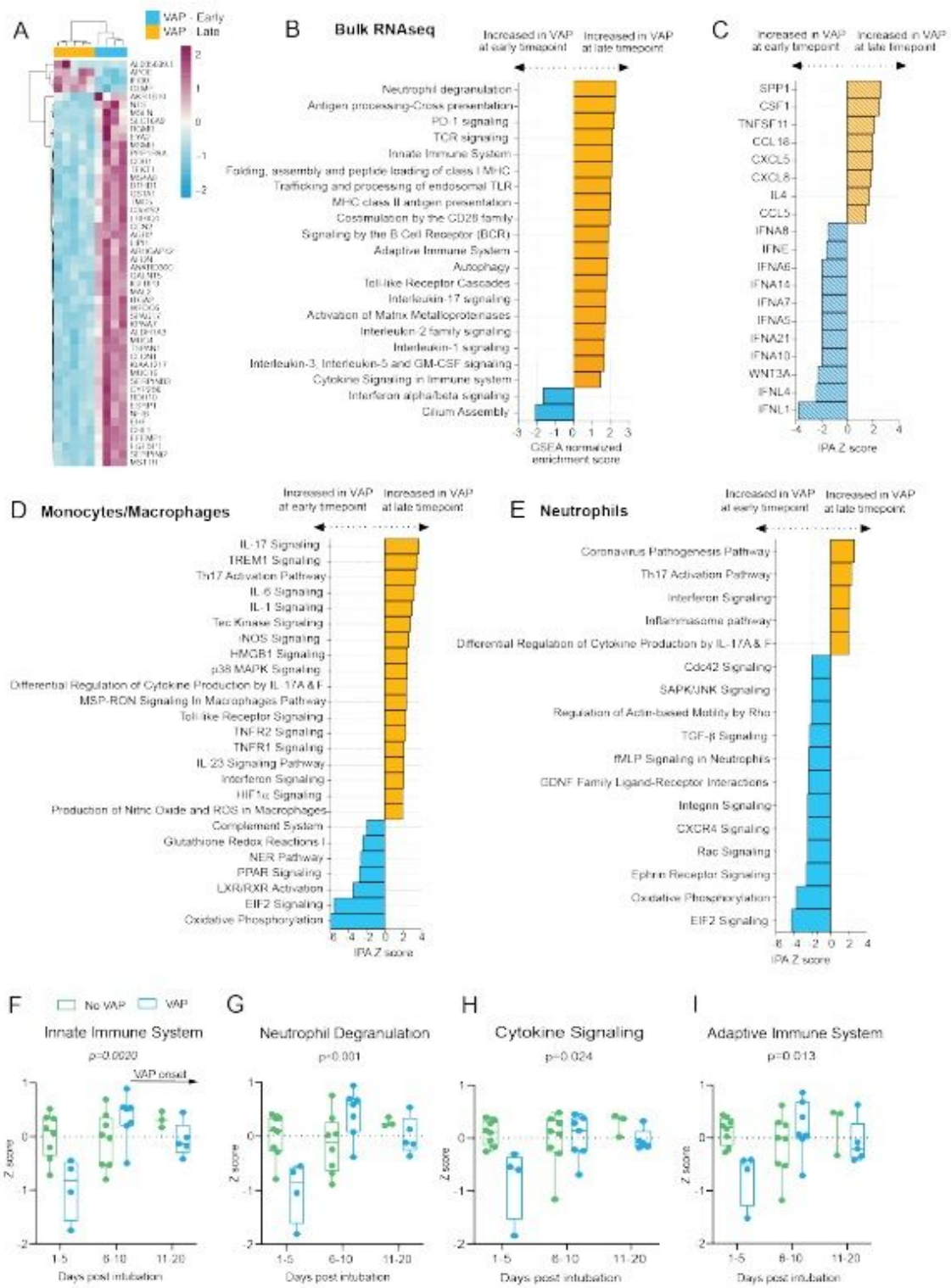


Figure 5

Temporal dynamics of the host response to VAP A) Heatmap of the top 50 differentially expressed genes by adjusted P-value between COVID-19 patients who developed VAP at the “early” time-point (blue) versus the “late” time-point (yellow) from bulk RNA-seq. B) Gene set enrichment analysis (GSEA) based on differential gene expression of VAP patients at the “early” vs “late” time-point from bulk RNA-seq. GSEA results were considered significant with an adjusted P-value <0.05 . C) Ingenuity Pathway Analysis (IPA)

of upstream cytokines based on differential gene expression analyses of VAP patients at the “early” vs “late” time-point from bulk RNA-seq. IPA results were considered significant with a Zscore absolute value >2 and overlap P-value <0.05. (D-E) Ingenuity Pathway Analysis (IPA) of key canonical pathways based on differential gene expression analysis in monocytes and macrophages (D) or neutrophils (E) from scRNA-seq of patients who develop VAP versus those who do not, with adjusted p-values < 0.05. Only significant pathways (IPA Z-score of >2 or <-2 and overlap p-value <0.05) are shown. All pathways and cytokines are shown in Supplementary data files 2, 3, 5, and 6. (F-I) Longitudinal analysis of selected pathway expression in VAP (blue) versus No-VAP (green) patients from bulk RNA-seq samples taken from time of intubation to onset of VAP for all patients. Pathway Z-scores were calculated by averaging Z-scores for the top 20 leading edge genes of each pathway, determined by the results of GSEA comparing VAP versus No-VAP patients at the “early” time-point. Multiple Z-scores per patient at a given time interval were averaged so that each patient corresponds to one datapoint at each interval. Samples from day 21+ after intubation are not shown due to a lack of these later time-points in the No-VAP group. VAP onset in these patients ranged from 10-39 days post intubation. Selected pathways are innate immune system (F), neutrophil degranulation (G), cytokine signaling (H), and adaptive immune system (I). Box plots represent the median and range. Statistical significance was determined by two-way ANOVA, and interaction p-values are shown.

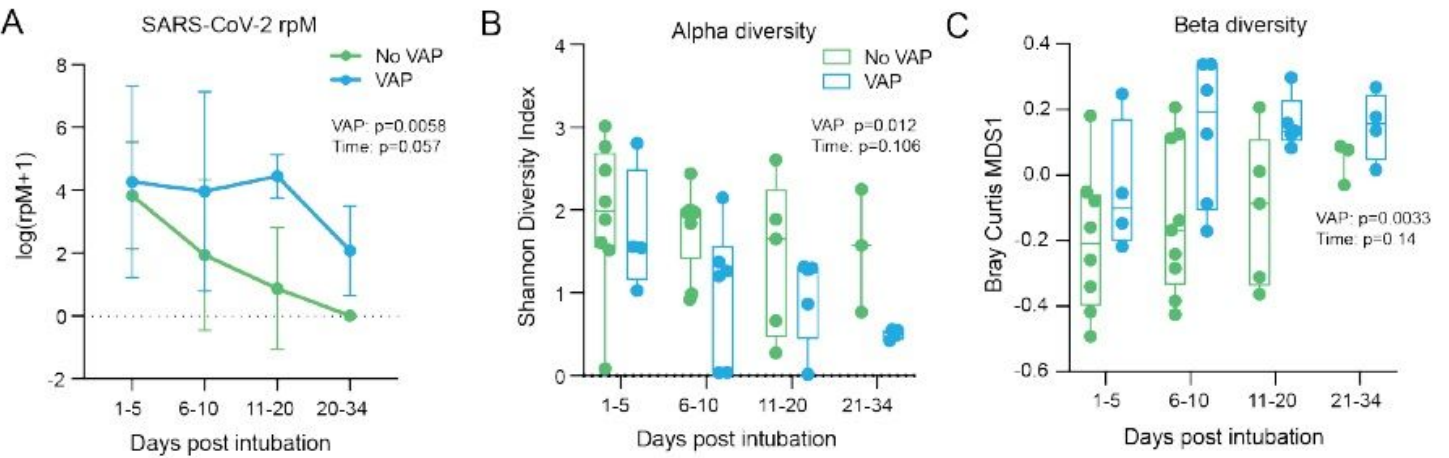


Figure 6

Lung microbiome community collapse precedes VAP in COVID-19 patients. (A) SARS-CoV-2 viral load (reads per million sequenced, rpM) over time by days since intubation in patients who develop VAP vs those who do not. For plotting purposes, $\log(\text{rpM}+1)$ was used to avoid negative values. Lung microbiome (B) bacterial diversity (Shannon’s Index) and (C) b-diversity (Bray Curtis Index, NMDS scaling) in COVID-19 patients with relation to VAP development over time by days since intubation. Box plots represent the median and range (AC). Statistical significance was determined by two-way ANOVA. P-values <0.05 were considered significant.

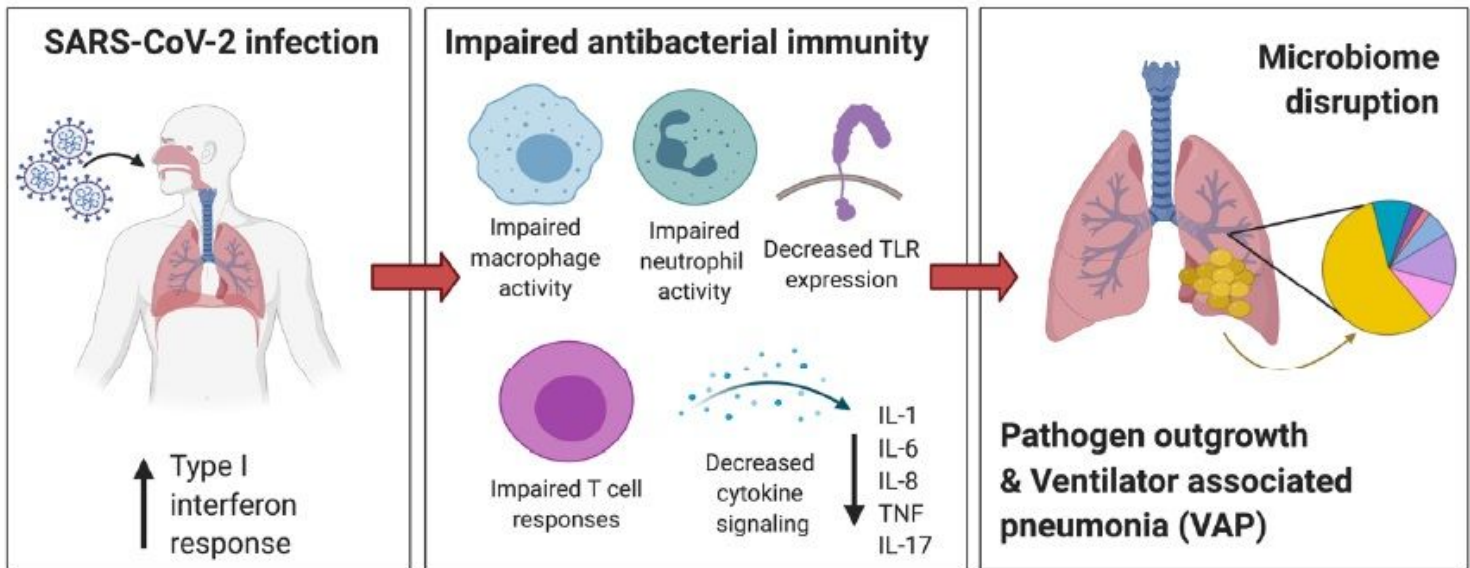


Figure 7

Mechanistic hypothesis of secondary bacterial pneumonia susceptibility in patients with COVID-19. Individual immune responses to SARS-CoV-2 infection drive a restructuring of the microbial community and increase susceptibility to VAP. Those predisposed to VAP have increased type I interferon responses and dysregulated antibacterial immune signaling characterized by impaired macrophage, neutrophil and T cell activity, decreased TLR signaling and impaired activation of key cytokines important for pathogen defense including IL-1, IL-6, IL-8, TNF, and IL-17. This state of suppressed immunity disrupts the lower respiratory tract microbiome, predisposing to outgrowth of bacterial pathogens and VAP.

Supplementary Files

This is a list of supplementary files associated with this preprint. Click to download.

- [SupplementaryAppendixCOMETConsortiumMemberlist.xlsx](#)
- [SupplementaryMaterialsNC3.31.2021.pdf](#)
- [DATAS1BulkRNAseqDEgenes.xlsx](#)
- [DATAS2BulkRNAseqFGSEA.xlsx](#)
- [DATAS3BulkRNAseqIPAUpstreamRegCytokines.xlsx](#)
- [DATAS4singlecellRNAseqDEgenes.xlsx](#)
- [DATAS5scRNAseqIPACanonicalPath.xlsx](#)
- [DATAS6scRNAseqIPAUpstreamRegCytokines.xlsx](#)
- [DATAS7PatientMetadata.xlsx](#)
- [nrreportingsummaryNCOMMS2112534.pdf](#)
- [nrsoftwarepolicyNCOMMS2112534.pdf](#)